EUROPEAN FUSION DEVELOPMENT AGREEMENT

EFDA–JET–PR(01)125

J.-M. Noterdaeme et al

Spatially Resolved Toroidal Plasma Rotation with ICRF on JET

Spatially Resolved Toroidal Plasma Rotation with ICRF on JET

J.-M. Noterdaeme[1], E.Righi[2], V. Chan[3], J. deGrassie[3], K. Kirov[1], M. Mantsinen[4], M.F.F.Nave[5], D. Testa[6], K-D. Zastrow[7], R. Budny[8], R. Cesario[9], A. Gondhalekar[7], N. Hawkes[7], T. Hellsten[10,11], Ph. Lamalle[10,12], F. Meo[1], F. Nguyen[13]
and JET-EFDA contributors*

[1] *Max-Planck-Institut für Plasmaphysik, Euratom Association, Garching, Germany,*
[2] *EFDA-CSU Garching, Germany,*
[3] *General Atomics, USA,*
[4] *Association Euratom-Tekes, Helsinki University of Technology, Finland*
[5] *Associacao Euratom/IST, Instituto Superior Tecnico, Lisbon, Portugal,*
[6] *Plasma Fusion Center, MIT, Cambridge, USA,*
[7] *UKAEA, Euratom Association, UK,*
[8] *PPPL, Princeton, USA,*
[9] *ENEA, Euratom Association, Frascati, Italy,*
[10] *EFDA-CSU JET, UK,*
[11] *NFR, Euratom Association, Sweden,*
[12] *Association Euratom-Belgian State, LPP-ERM/KMS, Belgium*
[13] *CEA Cadarache, Euratom Association, France*
** See annex of J. Pamela et al, "Overview of Recent JET Results and Future Perspectives", Fusion Energy 2000 (Proc. 18th Int. Conf. Sorrento, 2000), IAEA, Vienna (2001).*

Paper to be submitted for publication in Nuclear Fusion

ABSTRACT

ICRF only heated plasmas in the JET tokamak show distinct structures in the toroidal rotation profile, with regions where $d\omega/dr > 0$ when the minority cyclotron resonance layer is far off-axis. The rotation is dominantly co-current with a clear off-axis maximum. There is only a slight difference between a high field side or a low field side position of this resonance layer: the off-axis maximum in the rotation profile is modestly higher for the high field side position. This is in contrast to the predictions of theories that rely mainly on effects arising from ICRF-driven fast ions to account for ICRF-induced plasma rotation. The differences due to the direction of the antenna spectrum (co- or counter-) are small. A more central deposition of the ICRF power and operation in H-mode both lead to more centrally peaked profiles. Strong MHD modes break the rotation and lead to overall flat rotation profiles.

1. INTRODUCTION

Plasma rotation plays an important role in several areas: from transport, where shear in the rotation can lead to reduced transport losses, to MHD where rotation will increase the stabilizing effect of a resistive wall. Toroidal rotation is typically induced by momentum input through Neutral Beam Injection (NBI). This direct momentum input, if present, tends to dominate the toroidal force balance and can naturally lead to strong toroidal rotation.

In the absence of direct momentum input, or with negligible direct momentum input as in the case of RF heating, other mechanisms can lead, in a magnetized plasma, to rotation. Measurements have repeatedly shown that the application of significant RF power to a tokamak discharge can result in a change in the mean toroidal velocity of the measured ion. A special case is when RF-heated particles are driven out of the plasma, resulting in a radial current and a change in the plasma potential profile. Except for this case, there is not yet definitive experimental evidence whether or not the observed changes are due to plasma heating per se, modifications in momentum transport, or some RF effect reliant upon the specific aspects of the wave-particle interaction. For ICRF minority heating in particular, the radial transport of resonant ions as well as friction between them and the plasma can, for example, lead to a toroidal torque. Several such RF specific mechanisms have been proposed, leading to distinct predictions for the dependence of the toroidal rotation on a number of parameters, like the location of the resonance layer. A review on the subject is given in [1].

Theoretical predictions with sometimes contradicting results for the rotation profiles coexist in view of the scarcity of experimental data for plasmas not dominated by the direct momentum input from the neutral beam injection. Whereas rotation *profiles* have previously been recorded for the combination of NBI and ICRF, little information has been available on spatially resolved toroidal rotation *profiles* for ICRF only. Rotation profiles in the case of ICRF only, for various RF conditions (such as different positions of the resonance layer, and spectra) are the experimental basis needed to make further theoretical progress. It will allow better quantification and separation of the different components that can affect the toroidal rotation such as the plasma heating per se, modifications in

momentum transport, or RF specific effects. Such investigation is all the more important because it reproduces experimental conditions in the next step fusion experiment, where the toroidal momentum input, if present at all, will be substantially smaller than in current-day machines and fast particles will be dominantly present. An understanding of the momentum sources and of the momentum transport is urgently required.

The paper reports experiments [2, 3] with H minority heating in D, where for the first time on JET, spatially resolved toroidal rotation profiles were measured under conditions of no major external momentum input. The profiles were measured for various positions of the resonance layer, for various symmetric and asymmetric launched spectra, for different minority concentrations, for L and H mode. Though the experiment required 'blips' (short neutral beam pulse) to make measurements, care was taken to design the experiment such (and the measurements confirm) that the momentum and energy input due to this measurement did not significantly affect the results.
This paper is organized as follows: section 2 discusses the measurement methods, provides a review of previous observations of plasma rotation in discharges with RF and theoretical background. Section 3 presents the experiments: the experimental conditions, the measurement method, the conduct of the experiment, confirmation that the measurement method did not affect the results and the results. Section 4 analyses and discusses the results in view of the theories. Section 5 summarizes and concludes.

2. BACKGROUND ON TOROIDAL ROTATION

2.1. MEASUREMENT OF THE ROTATION

Rotation is typically measured using spectroscopic methods. The mean ion velocity and temperature can be measured by fitting a Doppler shifted Gaussian profile to the spectrum of atomic transition light emitted from a specific region of the plasma [47] for a given ion. In some cases, relatively high-Z ions are used which are not fully stripped in the interior of the hot plasma and emit photons from collisionally excited atomic transitions, usually in the X-ray region of the spectrum [5, 7]. In contrast, the technique of charge exchange recombination (CER) spectroscopy [4, 6, 8] used for the present experiments, looks at low Z ions. A fully stripped ion, such as C^{6+}, briefly receives an electron in an excited state by charge exchange with a neutral atom, coming from an injected neutral beam. The emitted light is in the visible range and the technique lends itself to a multi-channel profile diagnostic. However, with CER the neutral beam can provide a toroidal momentum source which can affect the measured ion velocity and this must be taken into account when designing experiments aiming at measuring the rotation in discharges nominally heated by RF only. Neoclassical theory is typically used to relate the toroidal velocity of the measured impurity to that of the bulk plasma ion [9]. In the absence of large bulk plasma pressure gradients, as may occur in high performance discharges with internal transport barriers, the difference in the toroidal velocities is not large [10]. Neoclassical theory was used to correct for the difference between the rotation of the C and the D for a number of discharges (see section 4.2), confirming that the differences are small.

2.2. PRIOR RESULTS ON TOROIDAL ROTATION

An early experiment on toroidal rotation with electron cyclotron heating (ECH) alone was done on Doublet-III using the high-Z technique with TiXXI [11]. Measurements from a number of discharges were taken over a period of time. In some cases there was a co-rotation in the Ohmic phase (of order 30 km/sec) which was 'braked' by the ECH. In other cases, there was no velocity in the Ohmic phase and with the ECH pulse a counter-rotation developed which turned around and became co-rotation, saturating at about 30 km/sec.

In TFTR experiments, RF-induced velocity changes have in some cases been clearly due to RF-heated particles driven out of the plasma, which drive a radial current and a change in the plasma potential profile It was demonstrated, by varying the resonance location in minority D(H) ICRH discharges, that the loss of fast ions could explain the strongest counter rotation (of order 50km/ sec) [12]. This experiment used ICRH alone and measured spectra from FeXXV.

Similarly, the loss of fast electrons is the explanation for an induced co-rotation in lower hybrid current drive (LHCD) discharges on JT-60U wherein the LHCD power was large enough to drive essentially all of the plasma current [13]. Here, diagnostic neutral beam 'blips' were used for CER measurements.

In JET, toroidal velocity measurements have been made for many years using both spectroscopic techniques, with comparisons between the high-Z and CER measurements. The X-ray crystal spectrometer (KX1) relied on emission from He-like nickel lines (in those times abundant during ICRF heating) and measured v_ϕ and T_i at one location in the plasma.

In an early the central rotation versus RF-power and fast energy content was analyzed with symmetric phasing [14]. A systematic increase of the rotation in the direction of the plasma current was seen both with the total RF-power and the fast energy content although the spread was rather large. The best correlation was seen with the fast energy content, not the RF-power. This analysis contained also off-axis heating but the rotation was low, consistent with little tail formation due to the low power density. Since only the center was measured, a change in the profile could not be studied. These experiments were conducted with limiter plasma and the rotation was not strong. The conclusion was that the observed effect essentially an RF effect, and not an heating effect.

Another set of experiments was made by Eriksson, Righi and Zastrow [15]. In ICRF only discharges with the MkI divertor a toroidal co-current velocity of 15-30 km/sec was measured in L-mode at about r/a = 0.3 from the plasma center with a value independent of P_{RF} as long as the plasma remained in L-mode [15]. The local toroidal angular momentum was found to be proportional to the local bulk ion pressure (n_iT_i), perhaps indicative of an effect not specific to RF. When the L-H transition occurred, the plasma started to accelerate and v_ϕ reached values (50 km/s) about a factor of three smaller than those obtained with NBI. Acceleration due to the H-mode was attributed to the pressure gradient.

A similar result has been found on C-Mod [7, 16]. Co-rotation is measured for ICRH only discharges with the increment in toroidal velocity (over Ohmic) found to be proportional to the plasma stored energy [7]. This proportionality was valid across L and H-mode regimes, with a maximum toroidal

velocity reaching about 100 km/sec. Subsequently, comparable toroidal velocities were measured in Ohmic H-modes with no ICRH [16], showing that the RF aspects are not a necessary condition. C-Mod measurements are made with ArXVII and ArXVIII spectral lines. More recently C-Mod has found that carefully positioned off-axis ICRH can induce a transition to an internal transport barrier with a reduction in and eventual reversal of the usual co-rotation following the transition [17].

In experiments in which the target discharge has toroidal velocity driven by neutral beam injection (NBI), the addition of RF power often reduces the magnitude of the toroidal velocity. Experiments on DIII-D have shown this to be the case with electron cyclotron heating (ECH), electron cyclotron current drive (ECCD), or fast wave current drive (FWCD) [18]. The FWCD system on DIII-D is designed to operate at the high ion cyclotron harmonic frequencies in order to maximize wave damping on electrons. Target discharge velocities are typically in the 100-500 km/sec range from NBI and can be reduced by up to 30% during the RF pulse. Ion temperature in the core is usually also reduced. The universality of the effect, independent of the details of the electron heating method have led to the hypothesis that the reduction is due to higher turbulent ion momentum and thermal transport with increased T_e/T_i [18].

This same particular effect has also been observed in certain JET discharges [5, 19]. Using emission from NiXXVII and additional impurity lines in the XUV, a "cooling and slowing down" with the application of an ICRF pulse was observed [5].

On TFTR this reduction in speed has been measured with CER for the addition of ICRH to both co and counter rotating target discharges indicating application of a drag, or enhanced momentum transport [20].

2.3. THEORETICAL MODELS FOR RF INDUCED PLASMA ROTATION

In this section, the theoretical background for plasma rotation and in particular the RF specific effects is summarized.

A variety of mechanisms can affect plasma rotation. They are represented in the flux-surface averaged toroidal momentum equation

$$M_i n_i \frac{d}{dt}\langle U_\phi R\rangle = -\frac{1}{c}\langle j_f \cdot \nabla\psi\rangle + \langle R\vec{e}_\phi \cdot F_c\rangle + \langle R\vec{e}_\phi \cdot F_w\rangle - \langle R\vec{e}_\phi \cdot (\nabla\cdot\Pi_i)\rangle \qquad (1)$$

Here, U_ϕ is the flow velocity with the subscript ϕ indicating the toroidal direction, F_C is the frictional force acting on the electrons and ions by the fast ions, F_W represents collisionless momentum input by the waves, and $< j_P \cdot \nabla\psi > \sim= - < j_f \cdot \nabla\psi >$ is used with j_P being the plasma current and j_F, the fast ion current. This term accounts for any mechanism that produces a radial particle current for fast ions, which imposes a j x B torque on the bulk plasma. The last term on the RHS is the toroidal component of the stress tensor and may be related to an empirical momentum confinement time τ_ϕ by setting

$$\langle R\vec{e}_\phi \cdot (\nabla \cdot \Pi_i) \rangle \approx M_i n_i \frac{\langle U_\phi R \rangle}{\tau_\phi} \tag{2}$$

Using Eq(2) in Eq(1) yields momentum balance on a local flux surface. We can also write the last term in differential form

$$\langle R\vec{e}_\phi \cdot (\nabla \cdot \Pi_i) \rangle \approx \frac{d}{dr} r \langle X_m \rangle \frac{d}{dr} M_i n_i U_\phi \tag{3}$$

which, when combined with Eq(1), can be solved for the toroidal rotation profile subject to appropriate boundary conditions and choice for the momentum diffusivity, X_m.

Depending on the physical mechanism under consideration, some terms on the RHS of Eq(1) may be more important than others. The F_w term would be dominant if there is direct momentum input by resonant [21] or non-resonant [22, 23] wave processes. The accretion theory of "spontaneous" rotation [24, 25] introduces a momentum source at the boundary, and unstable electrostatic waves supply a X_m as well as an inward pinch, leading to inward momentum transport.

For this paper, we shall focus on mechanisms related to ion cyclotron resonance heating (ICRH) of a minority ion species.

The effect of RF induced radial diffusion [26], and RF driven fast ion losses in the presence of a loss cone [27] have been investigated theoretically, both would lead to a torque in the counter-current direction consistent with earlier experiments.

One of the first theories to propose a mechanism for co-current rotation drive by ICRH [28] called attention to the effect of finite orbit width on both trapped and passing ions. A minority trapped ion heated by ICRH will preferentially expand its bounce-averaged radius outward resulting in a counter-torque, while passing ions heated by ICRH will preferentially drift inward resulting in a co-torque. Chang's paper argues that for Alcator C-Mod parameters, the passing particles dominate hence a co-rotation should occur. A Monte-Carlo orbit calculation illustrated the conclusion. However, the calculation did not account for the companion frictional torque imposed by the fast ions on the bulk plasma. This paper also states that pitch-angle scattering does not add significantly to the radial diffusion of the energetic particles. This contradicts another finite orbit theory [29] in which ion-ion pitch angle scattering is the dominant mechanism that leads to inward and outward radial diffusion of fast particles. The combination of magnetic (j x B) and frictional torque can generate a rotational profile even though the ICRH introduces negligible angular momentum. The central rotation is in the co-current direction when the resonance location is on the outboard (low-field) side of the tokamak, and counter-current direction with the resonance on the inboard (high-field) side. A Monte-Carlo drift orbit code was used in the simulation with the fast ions either provided by an initial mono-energetic distribution, or a simple model to "mock-up" the ICRH process.

Another study examined the mechanism proposed in [29] under the realistic condition when fast ions are continuously heated and slowed down in a driven system [30]. A quasilinear wave diffusion operator is implemented to simulate the heating process. When the heating geometry corresponding

to no net angular momentum is chosen, the result of [29] is reproduced for the case of zero parallel wavenumber $N_{//}$ (no Doppler resonance). The physical picture that emerges from this study is that the directionality of the rotation is a consequence of finite drift orbit width and RF-induced transport of the resonant ions. A study by [31] calculates a central co-rotation torque for the center where the inward drift dominates, indepently of the phasing, and a counter torque off-axis. In order to obtain for those torque the resulting rotation, the friction would have to be included. Very recently, Perkins has extended his study to treat rotation induced by traveling fast waves with a directed spectrum i.e. with parallel momentum input [32].

3. EXPERIMENTAL MEASUREMENTS

3.1. ICRF CONDITIONS

The experiments were conducted on the JET tokamak at a plasma current of 2 MA (clockwise as seen from the top of the tokamak and co-linear to B), and at various toroidal magnetic fields between 2.3 T and 3.2 T.

Several frequencies (nominally 37, 42, 51 MHz) at a constant magnetic field (2.8 T) were used to position the resonance layer of the H minority ($n_H / n_D = 0.005$-0.04) at specific locations (2.5 m $< R_{res} <$ 3.5 m) in the plasma. Alternatively, a ramp of the magnetic field (upward from 2.3 T to 3.1 T or downward from 3.1 T to 2.3 T) at constant frequency (42 MHz) moved the resonance layer from HFS to LFS or vice-versa during the discharge.

Note that, in JET, the four antenna arrays usually operate for technical reasons at slightly different frequencies. The nominally 37 MHz was in these experiments in fact 37.38 MHz, 37.37 MHz, 37.40 MHz, 37.30 MHz. Similarly 42 MHz was 42.47 MHz, 42.50 MHz, 42.24 MHz, and 42.25 MHz. And 51 MHz was 51.30 MHz, 51.30 MHz, 50.60 MHz, and 51.13 MHz. In addition, the frequency is used to match the antenna impedance and can vary in a discharge by ± 150 kHz. The exact power deposition thus depends on the power distribution between the arrays and on the matching. The maximum variation of 1 MHz at 51 MHz lead to an uncertainly of the resonance location of 5 cm. In the remaining text, the resonance locations are given for the nominal frequencies. Fig. 1 show the location of the power deposition for the resonance layer positioned at the high field side (B= 2.8 T, f= 51 MHz, R = 2.53 m) and at the low field side (B= 2.8 T, f= 37 MHz, R = 3.49 m), calculated using the SPRUCE [33] module in TRANSP (for $k_{//} = 6.9$ m).

Each of the four A2 antenna arrays in JET has four straps that can be phased arbitrarily. Symmetric spectra or asymmetric directed spectra can be chosen. The phasing used for the symmetric spectra were $(0, \pi, \pi, 0)$ or $(0, 0, \pi, \pi)$ or $(0, \pi, 0, \pi)$. The choice of the phasing $(0, \pi/2, \pi, 3\pi/2)$ results in co-directed spectra i.e. the wave is directed in the co-current direction. Counter-directed spectra are obtained with $(0, -\pi/2, -\pi, -3\pi/2)$. Typical spectra of the antenna current are shown in Fig.2.
Short pulses of D neutral beam injection 'blips' (E = 140 keV, Δt = 200 ms) were used to measure the plasma rotation profile using CXRS. It is shown in section 3.4 that the measurements did indeed measure the undisturbed rotation of the plasma (i.e as it was before the beam was injected) and not the rotation as affected by the beam.

In Fig. 3 typical electron temperature and density profiles (# 51668) are plotted at the time of the measurement in L-mode and in H-mode.

3.2. MEASUREMENT METHOD

The measurement of the toroidal rotation was deduced from the Doppler shift of the active charge-exchange (CX) spectrum of CVI [8]. A sketch of the geometry is shown in Fig. 4. The spectral dispersion of the instrument is calibrated for every discharge using the observed wavelength position of the "cold" BeII emission in the SOL, see Fig. 5. The wavelength position does not change during a discharge, which confirms that any toroidal rotation of the SOL is below the detection limit of the instrument.

The spectra can be analysed in two ways. The first method is to fit two Gaussian components to the CVI feature. The "warm" component is due to CX between C^{+6} ions and thermal deuterium at the edge. The "hot" component is the active signal from the intersection of the line-of-sight with the beams. The second method is to subtract spectra taken prior to application of NBI, and to analyse the difference spectrum with only one Gaussian component. The difference in the results in terms of observed Doppler shift and derived frequency of toroidal rotation is shown in Fig. 5.

The first method works well when there is a large difference between edge and core temperature and rotation because the two components are clearly distinguished from each other. However the plasmas of our study are difficult to analyse in this way, and we have chosen to select the subtraction method. Care has to be taken that the passive features are not changed when NBI is applied. Difference spectra with a residual spectral line (positive or negative) around BeII and CIII had to be rejected, since this is indicative of changes in the plasma edge. In the figures showing the rotation profiles, the time of the measurements are indicated as well as the time used for the spectrum which was subtracted.

A correction to the derived frequency of toroidal rotation is necessary because of the energy dependence of the CX cross sections [34]. The effect is due to ions moving towards the beam experiencing a larger cross section than those moving away from the beam. In JET this always results in a lower observed frequency of toroidal rotation. The magnitude of this effect is small in these plasmas due to the low ion temperature, with no correction for R>3.4 m, and rising to +2 krad/sec in the plasma centre, see Fig. 6.

3.3. EXECUTION OF THE EXPERIMENT

Fig. 7. shows the time evolution of a typical discharge. Both during the low ICRF power (2 MW), and during the high ICRF power (8 MW) phase of the discharge (this last phase is usually in H-mode) there is a sequence of 4 beam 'blips'. The first and the third are D beams with beam energy of 140 keV, used for the CXRS measurement, the second (80 keV) were intended for poloidal rotation measurement, the fourth (80 keV) for MSE. We only discuss here the toroidal rotation measurements.

In one series of experiments for the first and third 'blip' a beam with tangency radius of 1.31 m was used and a typical momentum input of 0.64 N/s (torque 1.31 x 0.64 Nm/s). In a second series of experiments, for the first and third 'blip' two beams were used with tangency radii of 1.85 m and total resulting torque of 2 x 1.85 x 0.64 Nm/s.

During each beam 'blip', spectra are measured every 50 ms, so that during each beam blip which last 200 ms, 3 to 4 spectra are recorded. In the figures that show the calculated rotation profiles, the 3 to 4 spectra taken during a beam blip are shown, with the first measurement in bold.

3.4. VERIFICATION OF THE MEASUREMENTS

Since the rotation measurements with CXRS need the neutral beam, and we want to investigate the rotation without external momentum, it is necessary to confirm that the toroidal rotation measurements (or which part of those measurements) are not influenced by the NBI momentum input.

Several approaches show convincingly that the first measurement during the first short beam blip, after a steady state period of a few confinement times, measures indeed the rotation as it was before the beam was turned on.

Information on this can be gathered from the analysis of the evolution itself of the rotation profile during one beam blip (three to four profiles can be recorded) and from one beam blip to another (with different timing).

From the evolution of rotation profiles during the first beam blip, we see that the rotation is (except for the center) little affected by the first beam blip (as seen in Fig. 8a). Further, we can compare the first rotation profile during the first beam blip with the first rotation profile in the third blip, in the absence (Fig. 8a and b) or presence (Fig. 9a and b) of a second beam blip. With the second beam blip present, the cumulative effect of the beam induced rotation due to the first and the second beam blips can be seen to significantly affect the complete rotation profile at the beginning of the third beam blip (see Fig. 9).

Looking now at the four profiles in the first beam blip alone, in Fig. 8a and Fig. 9a, we do notice that the central rotation changes the fastest. It is thereby advantageous that the time dependence of this central rotation can be followed continuously under certain conditions: in experiments where a mild central n=1 mode is present, the central rotation also shows up as a modulation of magnetic signals. This modulation can be followed continuously (whether or not beams are present). It can thus provide information on the time scale of the evolution of the central rotation due to the application of beam (Fig.10). From this, we see that after 50 ms, the central rotation is still little affected by the beam. Since it is the central rotation that is affected the fastest, we can conclude that the first measurement of the first beam blip depicts faithfully the rotation profile as it was before the turn on of the beam.

The central rotation measurement based on the rotation of the central n=1 mode, in addition provides an independent check of the absolute value of this central rotation. It is in good agreement with the measurement made using CXRS.

Note that discharges that are strongly affected by MHD modes (for example after a big sawtooth crash) show a very flat rotation profile, with overall low values of the rotation. This is indicative of a powerful braking effect due to the modes, and is discussed in section 3.5.3.

A third approach addresses the issue in a computational way. Fig. 11 shows the total torque due to the NBI and its different components [35], calculated with TRANSP. The torque due to the NBI is clearly strongly centrally peaked. It was shown in [35] that the time evolution of the central torque is compatible with this torque input, and that the first measurement is little affected.

In a second series of experiments, for technical reasons, two beams were used for the beam blip. Even though this leads to a faster evolution of the rotation at the center, similar arguments as above show that the first profile still represents well the rotation as it was before the beam input.

3.5. EXPERIMENTAL RESULTS

In this part we present the results on the rotation profiles for different experimental conditions: L-mode, variation of the position of the resonance layer, effect of antenna spectrum, of the hydrogen concentration, H-mode.

3.5.1. L mode, far off-axis location of the resonance layer, asymmetric spectrum:

Influence of the HFS or LFS position of the resonance layer and of the direction of antenna spectrum

A set of 4 discharges was used to investigate the influence on the toroidal rotation profiles of the position of the resonance layer (far off axis HFS and LFS), and the direction of the asymmetric spectrum (co- and counter-directed).

The magnetic field was 2.8 T, the location of the resonance layer was moved by the choice of the resonance frequency (51 MHz for HFS resulting in R_{res} = 2.53 m, and 37 MHz for LFS resulting in R_{res} = 3.49 m).

The coupled power is 2 MW (± 50 kW) in all shots. PION [36, 37] calculations indicate that H minority absorption is in all cases dominant (between 75 and 85 %, depending on the resonance location, see also section 4.1).

Fig. 12 a and b shows the rotation profile for a HFS location of the resonance layer, for a co- and counter directed spectrum, and fig. 12 c and d for a LFS location, again for both spectra.
The overall rotation in L-mode with only ICRF, is smaller than with neutral beam injection. Whereas the profiles dominated by neutral injection are monotonically decreasing from the center to the edge, the profiles with ICRF only show more distinct structures.

For ease of direct comparison, figure 13 shows the first profiles only of each combination (LFS, HFS, co-, counter-spectrum).

Both for the LFS and the HFS position of the resonance layer, the rotation profiles have a clear maximum of co-rotation off-axis. This maximum is, for a HFS position as compared to the LFS position, slightly narrower and higher. There is some indication that it may be somewhat shifted to larger r/a.

The difference in rotation between the co- and counter spectra seems is most marked in the center. For both positions of the resonance layer, the central rotation for a co-spectrum is somewhat smaller than for a counter-spectrum. Note that the derived counter rotation in the center seen for the co-spectrum is due to the cross section effect discussed in section 3.2. The true rotation is larger than the apparent rotation by 2 krad/s. Therefore, in reality, the plasma is not rotating within the statistical error of ±1 krad/s. Since for the same reason, the true rotation is larger for the counter-spectrum by 2 krad/s, the difference between the rotation for the two directed spectra remains and is outside of the error bars.

Another result tends to confirm that the difference between co- and counter-directed spectrum is independent of whether the off-axis position of the resonance layer is on the HFS or LFS. In discharge with simultaneously a HFS position of the resonance layer (with a co-launched spectrum) and a LFS position of the resonance layer (with a counter-launched spectrum), the rotation profile is very similar to the rotation profile in a discharge with the opposite spectra (HFS resonance with the counter-launched spectrum and a LFS with a co-launched spectrum). (see figure 14).

3.5.2. Other phasings

In 3.5.1, we gave the comparison of co- and counter- phasing for a HFS as well as for a LFS position of the resonance layer. Cases with more phasings (including those resulting in different symmetric spectra) can be seen in Fig. 15. For a somewhat more central position of the resonance layer, but still HFS (R = 2.70 m, with f = 42 MHz, B = 2.45 T), the rotation profiles are shown (a) for a co- spectrum (0, π/2, π, 3π/2), (b) for a symmetric spectrum with (0, π, π, 0), (c) for a counter spectrum†(0, –π/2, –π, –3π/2), and (d) for a different symmetric spectrum†(0, π, 0, π). All the spectra are less hollow in the center, a consequence (see also 3.5.3) of the more central position of the resonance layer. The differences between the different spectra are small.

3.5.3. Other positions of the resonance layer

As can already be seen by comparing the far off-axis HFS position of the resonance layer (fig. 12 a, R = 2.53 m, f= 51 MHz, B = 2.8 T) with the more central position (fig 15 a, R = 2.70 m, f= 42 MHz, B = 2.45 T), a more central position of the resonance layer leads to an increase of rotation in the co-direction in the center. Both cases used the same co-spectrum. There is a slight difference in the H concentration (0.5 % for fig. 12a vs 2 % for fig 15a) and in the number of beams used in the blip (1 beam for fig12a and 2 beams for fig. 15a), which should however not affect the first measurement. An alternative comparison, from a series with the same number of beams and the same H concentration can be seen in Fig. 16. Both are from identical discharges with f = 42 MHz and symmetric spectrum (0,π,π,0). During each discharge, the magnetic field was ramped, and the measurements were taken at different times. For Fig 16 a the magnetic field at the time of the measurement was 2.33 T corresponding to R = 2.59 m and for fig 16 b the magnetic fieldwas 2.48 T (corresponding to R = 2.73 m). This comparison confirms the observation that a more central position of the resonance layer leads to a more peaked rotation profile.

An interesting observation resulted from the further evolution of the rotation profiles due to the variation of the resonance layer and comparing those with the values obtained for a fixed position of the resonance layer. Fig 17 shows in (b) the rotation profiles for conditions where the magnetic field was fixed (2.8 T), and the resonance located either on the HFS or on the LFS by choosing the appropriate frequency in different shots. The resonance layer was fixed at R = 2.53 m (HFS, f = 51 MHz) and R = 3.49 m (LFS, f = 37 MHz). In contrast to this, in (a) the resonance layer is varied from HFS to LFS, at fixed frequency (f= 42 MHz) by increasing the magnetic field from 2.3 T to 3.1 T. The results are shown for HFS (R = 2.59 m) and LFS (R = 3.17 m). Similarly to fig. 17 (a), in fig. 17 (c) the magnetic field in varied, but in the opposite direction, from LFS to HFS, by decreasing the magnetic filed (from 3.1 T to 2.3 T) at constant frequency (42 MHz). The results are shown for R = 3.08 m LFS and R = 2.58 m HFS. As the resonance layer location becomes more central, the hollowness of the rotation profile decreases. But, whereas the shape of the profile for the HFS case is similar for fig. 17 a and b (taking into account that the profile in (a) is somewhat more peaked because of the more central location) it is completely different for (c). Similarly for the LFS, the profiles in (b) and (c) are similar, but completely different from those in (a). The explanation is the following : when the resonance is moved from HFS to LFS of vice-versa by changing the magnetic field, the resonance passes at one point through the center. In those cases the sawteeth are stabilized and after a big crash strong MHD modes appear. Following their appearance, the rotation profile become very flat as the MHD modes break the rotation [38].

3.5.4. Influence of the concentration

Though no systematic scan of the concentration was done, the H concentration was different in two series of discharges performed on different days (1 +/- 0.5 % and 3 +/- 0.5 %). For a far off-axis position of the resonance layer (HFS), an increase in H concentration reduces slightly the off-axis co-rotation peak from typically 6 krad/sec to 5 krad/sec.

This can be seen in fig. 18. Fig 18 (a) and (b) shows for a far off-axis HFS position of the resonance layer (51 MHz, 2.8 T, R= 2.53 m) and a low H concentration (1 %) the rotation profiles for a co- and counter spectrum, whereas (c) and (d) show, for the same position of the resonance layer the profiles for a higher H concentration (3 %) and a symmetric (0, π, π, 0) spectrum. Note that the measurement in fig. 18 (d) was done with two beams which leads to the faster change of the profile from one measurement to the other.

3.5.6. H-mode

In H-mode, the rotation profile becomes more peaked (Fig. 19). The fast evolution seen in Fig.19 from one profile to the next (within the 200 ms blip) is partly due to the development of the H-mode, but in this case also to the larger beam power used in the blip.

4. ANALYSIS AND DISCUSSION

The theoretical studies discussed in section 2.3 illustrate the possibility of driving a rotation with ICRH with negligible momentum input. For theories that rely on fast particle effects to drive this rotation, the position of the resonance layer, the antenna spectra and the energy of the particles play a dominant role. We analyze therefore here in more detail specifically the discharges presented in section 3.5.1. where the position of the resonance layer and the spectrum was varied. We calculate the power deposition profiles and the energy of the fast particles. We further address the correction needed between the rotation of the measured ion (C) and of the bulk ions (D). Finally, we touch base with theory.

4.1. POWER DISTRIBUTION

For the discharges with a far off axis position of the resonance layer (HFS and LFS) and with a co- and counter spectrum, PION [36, 37] calculations were made to obtain in detail the power distribution between the different species and the power deposition profiles. H minority absorption is in all cases dominant, with about 1.5MW (75 %) for the HFS resonance cases and about 1.7 MW (85 %) for the LFS resonance cases. In the HFS case, the direct electron absorption (electron Landau damping and transit time magnetic pumping), is 400 kW (20 %), which is about 200 kW higher than in the LFS cases (200 kW = 10 %). The remaining power in both cases (100 kW = 5 %) is the power absorbed by the second harmonic damping on the deuterium. Fig. 20 (a) and 20 (b) show the profiles of power absorbed by hydrogen and direct electron damping respectively. The small radial shift in the hydrogen absorption profiles between discharges 51664-51665 with a HFS resonance, and discharges 51666-51667 with a LFS resonance, is due to an asymmetry in the resonance locations with respect to the center.

To obtain information on the location and energy of the fast ions, which play an important role in the theories, the discharges were modeled with the 3D Monte Carlo ICRF modeling code FIDO [39], which takes into account the ICRF induced transport of the fast protons. The radial total energy density and the mean energy of protons given by FIDO are shown in Fig. 21 and Fig. 22, respectively. Two sets of FIDO simulations are shown. In the first set, the measured background plasma parameters (including the measured variation of the H concentration) of the individual shots have been used. In the second set, the measured data of discharge 51664 have been used for all discharges in order to eliminate variations due to (small) differences in the background plasma parameters for the different discharges. The radial profiles of the proton energy density are similar, with maxima between r/a = 0.5-0.7, in all discharges.

The somewhat higher peak fast proton pressure given by FIDO for discharge 51666 than for the other discharges is attributed to the ICRF-induced transport of fast protons [40]. According to the FIDO simulations, the fraction of trapped fast protons increases from about 45% to about 65% of the total fast protons when the resonance is moved from the HFS to the LFS.

The total H energy content is about 40-50 kJ in all cases.

4.2. CORRECTIONS BETWEEN THE ROTATION OF C AND OF D

The neoclassical moment approach of Hirshman and Sigmar [41] is used to infer the toroidal rotation frequency of the main ion species (deuterium) from that measured for the impurity ions (carbon). These differ significantly in the regions of the plasma where the second radial derivative of the ion temperature is large, which is the case for an Internal Transport Barrier or edge pedestal [42]. The differential toroidal rotation velocity between the main ion species and the impurity ion species $\Delta V_\phi = V_{\phi D} - V_{\phi C}$ is given by

$$\Delta V_\phi = \frac{V_{thD}\,\rho_{\theta D}}{4 L_{TD}} \left[K_2 \left(1 - \frac{3B_\phi^2}{< B^2 >} \right) - \frac{L_{TD}}{L_{pD}} \left(1 - \frac{Z_D T_C}{Z_C T_D} \frac{L_{TD}}{L_{pC}} \right) \left(1 - \frac{B_\phi^2}{< B^2 >} \right) \right] \qquad (4)$$

Here V_{th} and ρ_θ are the ion thermal speed and poloidal gyroradius; Z and T are the ion nuclear charge and temperature, and we have assumed equal temperature for the impurity and the main ion species, $T_D = T_C = T_i$. The pressure scale length L_p is related to the temperature and density scale lengths L_T and L_n by $1/L_p = 1/L_T + 1/L_n$, where $1/L_T = d(\ln T)/dr$: thus the scale length is negative for a quantity decreasing with the minor radius r. The collisionality parameter K_2 is given in [9] B_ϕ and $<B^2>$ are respectively the local toroidal and flux-surface averaged magnetic field. Figures 23, 24, 25 and 26 shows the corrections needed between the toroidal rotation of D and C. The corrections are small and the differences between the corrections for the 4 discharges even smaller, so that we can discuss the rotation profile of the C.

4.3. COMPARISON WITH THEORY

Whereas a comparison of the experiments with individual theories clearly is beyond the scope of this paper, it is worth pointing out in which areas the measurements gives results different from the theoretical expectations.

A first aspect is the dominant co-direction of the rotation. Some theories reviewed in 2.3 predict a counter-torque as a result of the RF induced radial diffusion of RF driven fast ion losses. However, they cannot explain the co-current rotation observed in the experiments on Alcator C-Mod [43] or in the experiments on JET reported in this paper. One explanation could be that the RF specific effects are only partially responsible for the observed rotation. Budny [35] has argued that a significant co-rotation at the edge is generated by the loss of ions near the x-point.

Ohmic cases indeed show a rotation in the co-direction, and there is some indication that this is influenced by the distance between the x-point and the septum. This may indeed lead us to the conclusion that the shape of the profile is more likely due to a *counter central* torque (for both HFS and LFS off-axis) rather than an *off-axis co* torque.

On the other hand, the narrower profile and its shift towards larger r/a in the HFS case is consistent with the power deposition in the HFS case, which is narrower and slightly shifted towards larger r/a.

A second aspect is the small difference between the HFS and LFS position of the resonance layer, whereas a more central position of the resonance layer clearly behaves differently. Most of

the theories, that rely on fast particle effects predict an opposite direction of the torque for a HFS or a LFS position of the resonance layer. A HFS position of the resonance layer leads to a counter-torque and a LFS to a co-torque. None of those theories provide a basis for the co-rotation observed with the resonance on the inboard side. Even if the rotation is due to a superposition of effects, as argued above, a difference should still be seen between the HFS and the LFS position of the resonance layer. The differences are however small. Recently, continuing their simulation of a driven system, Chan [44] found that with finite $N_{//}$ (Doppler resonance accounted for), even in the absence of parallel momentum input, a net torque in the co- (counter-) direction is produced with positive (negative) $N_{//}$ for both inboard and outboard side resonance.

This is explained by the preferential production of co- (counter-) moving fast ions. Though it could offer a possible explanation of co-rotation in ICRH plasmas with high-field side resonance for a positive $N_{//}$, or even for a symmetric launched (if in the plasma a mechanism favours positive $N_{//}$), the small difference between the co- and counter- spectra in the experiment rules out this possibility as the major reason for the rotation in the co-direction for a HFS position of the resonance layer. A possible explanation could involve a preferential excitation of positive $N_{//}$, in the plasma even when the launched spectrum has a dominant negative $N_{//}$ component. Because of the rotational transform, the magnetic field is not aligned with the symmetry axis of the antenna. Preliminary antenna coupling analysis indicates that under some conditions, namely when the density in front of the antenna is high and the antenna current distribution is such that significant high poloidal mode numbers are excited, the power spectrum launched into the plasma can have a strongly asymmetric spectrum that favors positive $N_{//.}$ It remains to be determined whether this is the case on JET or Alcator C-Mod and more detailed comparisons will be required to test the model.

The difference between the two directed spectra (co- counter) seem to be more consistent than the difference between the HFS and LFS position of the resonance layer.

In terms of a counter torque at the center, it would mean that for the co-directed spectrum this counter torque would be slightly larger (in absolute value) than for a counter directed spectrum, independently of the position of the HFS or LFS localization of the resonance layer.

The small differences observed in the rotation profiles for a off-axis position of the resonance layer (HFS, LFS, co- or counter- spectrum) is thus an unexpected result of the present experiments. As we have shown in.section 4.2, the heating related parameters (except for the localisation of the energetic particles and the amount of trapped particles) are the same for both position of the resonance layer.

This would lead to the conclusion that the energetic particle effects (through their localisation) do not play the role they are given in the theories in producing most of the rotation.
Even when we assume that another mechanism produces the bulk of the rotation and that the ICRF produces variations on this, the differences are small, and more related to the spectrum than to the resonance layer.

5. SUMMARY AND CONCLUSIONS

The rotation in L-mode with only ICRF is smaller than with neutral beam injection.
But, whereas the profiles dominated by the neutral injection momentum input are monotonically decreasing from the center to the edge, profiles with ICRF only, show different structures depending on the position of the resonance layer, the presence of MHD modes or the status of the plasma (L-mode or H-mode).

For an off-axis position of the resonance layer, clearly non-monotonic†"hollow" profiles (with regions where $d\omega/dr > 0$) are seen. The distinct off-axis maximum in the co-current direction is seen for a far off-axis position of the resonance layer (HFS, R = 2.5 m or LFS, R =3.5 m). For the high field side position of the resonance layer, the off-axis maximum is modestly (20 %) higher than for the low field side position. The differences due to the direction of the antenna spectrum (co or counter – meant is the direction of the wave in relation to the plasma current) are small but consistent. If the hollowness of the rotation profiles for a far off-axis location of the resonance layer is interpreted as due to a central counter-torque, on top of an overall co-rotation, then there are some indications that this torque may be slightly larger (in absolute value) for a co-direction launch of the wave. It does not seem to be dependent on whether the resonance layer is far on the high field side or the low field side.

Those result would indicate that the fast particles do not play a significant role in the production of the rotation, in contrast to the prominent role they are given in many theories.

ACKNOWLEDGEMENTS

This work has been performed under the European Fusion Development Agreement.
It is a pleasure to acknowledge the dedicated work of A. Bickley, Y. Baranov, S. Conroy, C.Gowers, J. Mailloux, D. McDonald, S. Podda as session leaders and diagnostic coordinators.

* see appendix of J. Paméla, "Overview of recent JET results", Proceedings of the 18th IAEA Conference on Fusion Energy, Sorrento, 2000.

REFERENCES

[1] Chan V.S., ''Plasma rotation induced by RF'', *Radio frequency power in plasmas,* (13th Topical Conf., Annapolis, 1999), Vol. 485, (S. Bernabei ed. AIP, Melville, N.Y. (1999) 45.

[2] Noterdaeme J.-M., Righi E., deGrassie J. et al., ''Spatially resolved plasma rotation profiles with ICRF on JET'', *Radio Frequency Power in Plasmas,* (14th Topical Conf., Oxnard, CA, 2001), Vol. 595, (T.K. Mau and J. deGrassie eds.), AIP (2001) 98.

[3] Noterdaeme J.-M., Righi E., deGrassie J. et al., ''Toroidal plasma rotation with ICRF on JET'', *Plasma Physics and Controlled Fusion,* (28th EPS Conf., Madiera, Portugal, 2001), (2001) P2.080.

[4] Groebner R.J., Burrell K.H., Gohil P., and Seraydarian R.P., ''Spectroscopic study of edge poloidal rotation and radial electric fields in the DIII-D tokamak (invited)'', Rev. Sci. Instrum. 61 (1990) 2920.

[5] Mattioli M., Ramette J., Saoutic B. et al., ''Impurity ion temperature and toroidal rotation velocity in JET from high-resolution x-ray and XUV spectroscopy'', J.Appl.Phys. 64 (1988) 3345.

[6] Hawkes N.C. and Peacock N.J., ''Toroidal rotation in the dite tokamak'', Nuclear Fusion 25 (1985) 971.

[7] Rice J.E., Greenwald M.J., Hutchinson I.H. et al., ''Observations of central toroidal rotation in ICRF heated Alcator C-Mod plasmas'', Nuclear Fusion 38 (1998) 75.

[8] Weissen H., von Hellermann M., Boileau A. et al., ''Charge exchange spectroscopy measurments of ion temperature and toroidal rotation in JET'', Nuclear Fusion 29 (1989) 2187.

[9] Kim Y.B., Diamond P.H., and Groebner R.J., ''Neoclassical poloidal and toroidal rotation in tokamaks'', Phys. Fluids B 3 (1991) 2050.

[10] Kim J., Burrell K.H., Gohil P. et al., ''Rotation characteristics of main ions and impurity ions in H-Mode tokamak plasma'', Physical Review Letters 72 (1994) 2199.

[11] Lieber A.J., Snider R.T., Lee P., and Wojtowicz S.S., ''Electron cyclotron heating correlation with tokamak toroidal plasma rotation'', Phys. Fluids 31 (1988) 687.

[12] Hsuan H., Bitter M., Phillips C.K. et al., ''ICH-induced Plasma Rotation on TFTR'', *RF Power in Plasmas,* (11th Topical Conf., Palm Springs, 1995), Vol. 355, AIP (1995) 39.

[13] Koide Y., Tuda T., Ushigusa K. et al., ''Spontaneous plasma rotation of near-perpendicular neutral beam injection and lower hybrid current drive plasmas in JT-60U'', *Plasma Physics and Controlled Nuclear Fusion Research,* (14th Conf., W¸rzburg, 1992), IAEA 777.

[14] Eriksson L.-G., Gianella R., Hellsten T. et al., ''Observations of Toroidal Plasma Rotation Induced by ICRH in JET'', Plasma Phys. Contr. Fusion 34 (1992) 863.

[15] Eriksson L.-G., Righi E., and Zastrow K.-D., ''Toroidal rotation in ICRF-heated H-modes in JET'', Plasma Phys. Control. Fusion 39 (1997) 27.

[16] Hutchinson I.H., Rice J.E., Granetz R.S., and Snipes J.A., ''Self-Acceleration of a Tokamak Plasma during Ohmic H Mode'', Physical Review Letters 84 (2000) 3330.

[17] Rice J.E., Boivin R.L., Bonoli P.T. et al., ''Observation of impurity toroidal roation suppression with ITB formation in ICRF and ohmic H mode Alcator C- Mod plasmas'', Nuclear Fusion 41 (2001) 277.

[18] deGrassie J.S., Baker D.R., Burrell K.H. et al., ''Toroidal Rotation and Core Ion Confinement with RF Heating in DIII-D'', *Controlled Fusion and Plasma Physics,* (26th EPS-Conf., Maastricht (NL), 1999), (1999) P3.064.

[19] O'Brien D.P., Balet B., Deliyanakis N. et al., ''Effect of shear in the radial electric field on confinement in JET'', *Controlled Fusion and Plasma Physics,* (21th EPS Conf., Montpellier (F), 1994), Vol. 18B, (1994) I.

[20] Phillips C.K., Bell R., Bernabei S. et al., ''Effects of ICRF waves on plasma rotation in TFTR'', Bull. American Phys. Soc. 42 (1997) 1972.

[21] Lin-Liu Y.R., Chan V.S., and Chiu S.C., ''Plasma Rotation in the Presence of Radio Frequency Fields'', *Radio Frequency Power in Plasmas,* (11th Topical Conf., Palm Springs, CA, 1995), Vol. 355, AIP (1995) 247.

[22] Chan V.S. and Chiu S.C., ''Plasma rotation in RF heated plasmas'', *Theory of Fusion Plasmas,* (Proc. Joint Varenna-Lausanne Int. Workshop, Varenna, 1994), Vol. ISPP-15, (1994) 89.

[23] Berry L.A., Jaeger E.F., Azevedo E.F.D. et al., ''Analysis of IBW-Driven Plasma Flows in Tokamaks'', *Fusion Energy,* (18th IAEA Conf., Sorrento, 2000), IAEA (2000) paper THP 2/24.

[24] Coppi B., ''Accretion Theory of ''Spontaneous'' Rotation in Toroidal Plasmas'', *Fusion Energy,* (18th IAEA Conf., Sorrento, 2000), (2000) THP 1/17.

[25] Coppi B., ''Accretion theory of 'spontaneous' rotation in toroidal plasmas'', Nuclear fusion 42 (2002) 1.

[26] Chiu S.C. and Chan V.S., ''Neoclassical transport in the presence of radiofrequency fields'', Nuclear Fusion 29 (1989) 1907.

[27] Chan V.S., Chiu S.C., and Wong S.K., ''Impurity transport in ICRH tokamak plasma'', Nuclear Fusion 25 (1985) 697.

[28] Chang C.S., Boloni P.T., Rice J.E., and Greenwald M.J., ''A theoretical model for the generation of co-current rotation by radio frequency heating observed on Alcator C-Mod'', Physics of Plasmas 7 (2000) 1089.

[29] Perkins F.W., White R.B., Bonoli P.T., and V.S. C., ''Generation of plasma rotation in a tokamak by ion-cyclotron absorption of fast AlfvÈn waves'', Physics of Plasmas 8 (2001) 2181.

[30] Chan V.S., Chiu S.C., and Omelchenko Y.A., ''RF-driven Radial Current and Plasma Rotation in a Tokamak'', Phys. Plasmas 9 (2002) 501.

[31] Hellsten T., Hedin J., Carsson J. et al., ''Effects of finite drift orbit width and Rf-induced spatial transport on plasmas heated by ICRF'', *Radio Frequency Power in Plasmas,* (14th Top. Conf., Oxnard, CA, 2001), AIP Conference Proceedings Vol. 595, (T.K. Mau and J. deGrassie eds.), AIP (2001) 377.

[32] Perkins F.W., White R.B., and Chan V.S., ''On plasma rotation induced by traveling fast Alfvén waves'', Physics of Plasmas 9 (2002) 511.

[33] Evrard M., Ongena J., and Van Eester D., ''Improved dieletric tensor in the ICRF module of Transp'', *RF Power in Plasmas,* (11th Topical Conf., Palm Springs, 1995), AIP Conference Proceedings Vol. 355, (R. Prater and V.S. Chan eds.), AIP (1995) 235.

[34] von Hellermann M., Berger P., Frieling J. et al., ''Analytical approximation of cross-section effects on charge exchange spectra observed in hot fusion plasmas'', Plasma Physics and Controlled Fusion 37 (1995) 71.

[35] Budny R.V., Chang C.S., Giroud C. et al., ''Comparison of theory with rotation measurements in JET ICRH plasmas'', *Plasma Physics and Controlled Fusion,* (28th EPS Conf., Madeira, Portugal, 2001), (2001) P2.001.

[36] Eriksson L.-G., Hellsten T., and Willén U., ''Comparison of time dependent simulations with experiments in ion cyclotron heated plasmas'', Nuclear Fusion 33 (1993) 1037.

[37] Eriksson L.-G. and Hellsten T., ''A Model for Calculating ICRH Power Deposition and Velocity Distribution'', Physica Scripta 52 (1995) 70.

[38] Lazzaro E., Hender T.C., Zanca P., and EFDA-JET, ''Anomalous braking and shear modification of plasma rotation in a tokamak'', *Plasma Physics and Controlled Fusion,* (29th EPS Conference, Montreux (CH), 2002), EPS (2002)

[39] Carlsson J., Eriksson L.-G., and Hellsten T., ''FIDO, a Code for Calculating the Velocity Distribution Function of a Toroidal Plasma during ICRH'', *Theory of Fusion Plasmas,* (Proc. Joint Varenna-Lausanne Int. Workshop, Varenna, 1994), Vol. ISPP-15, Editrice Compositori, Bologna (1994) 351.

[40] Chen L., Vaclavik J., and Hammett G.W., ''Ion radial transport induced by ICRF waves in tokamaks'', Nuclear Fusion 28 (1988) 389.

[41] Hirshman S.P. and Sigmar D.J., ''Neoclassical transport of impurities in tokamak plasmas'', Nuclear Fusion 21 (1981) 1079.

[42] Testa D., Giroud C., Fasoli A. et al., ''On the measurement of toroidal rotation for the impurity and the main ion species on the Joint European Torus'', Physics of Plasmas 9 (2002) 243.

[43] Rice J.E., Bonoli P.T., Goetz M.J. et al., ''Central impurity toroidal rotation in ICRF heated Alcator C-Mod plasmas'', Nuclear Fusion 39 (1999) 1175.

[44] Chan V.S., Chiu S.C., and Omelchenko Y.A., ''Doppler resonance effect on rotational drive by ion cyclotron minority heating'', *APS-DPP Meeting,* (43rd Annual Meeting, Long Beach, CA, 2001), General Atomics (2001) paper KP1.037.

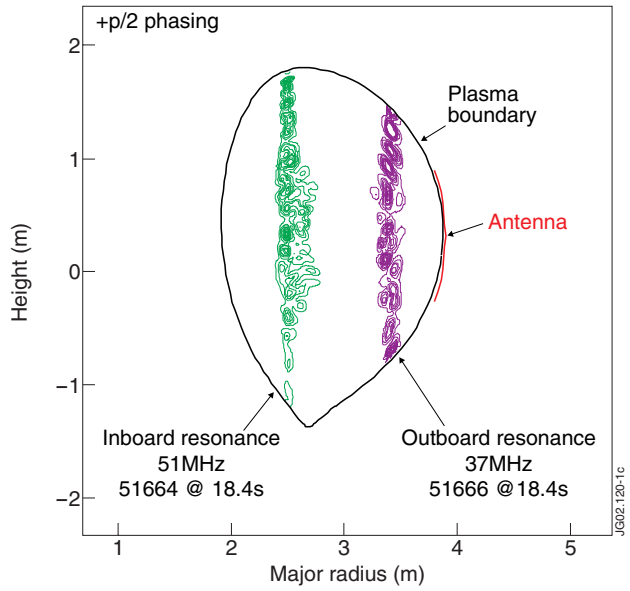

Figure 1: Location of the power deposition for the resonance layer positioned at the high field side (B= 2.8 T, f= 51 MHz) and at the low field side (B= 2.8T, f= 37 MHz), calculated using the SPRUCE module in TRANSP

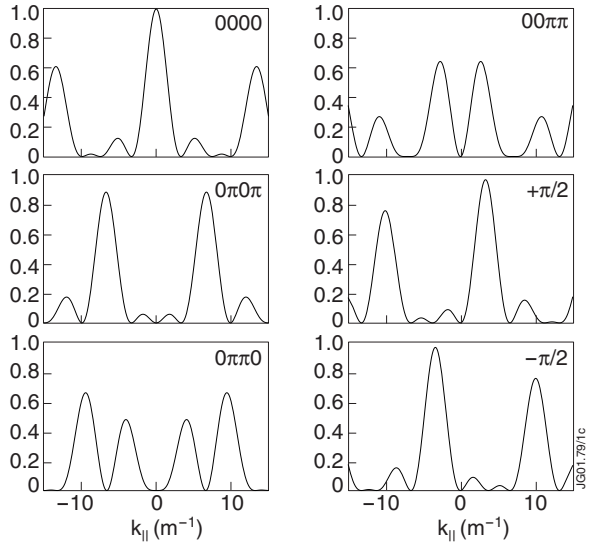

Figure 2: Toroidal spectra of the antenna currents for various phasings. Note that the spectrum seen by the plasma may be different, depending on the edge density.

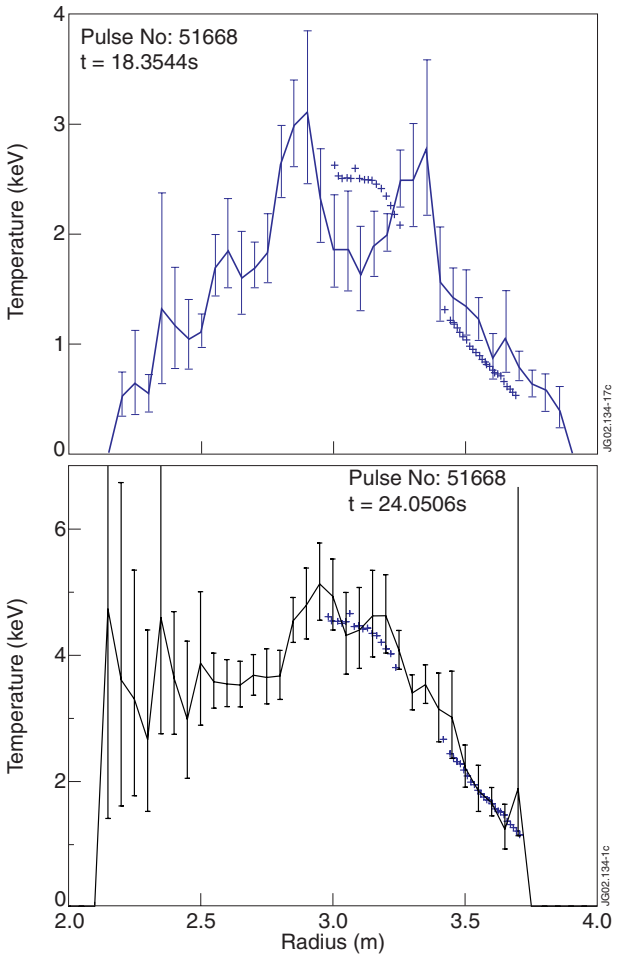

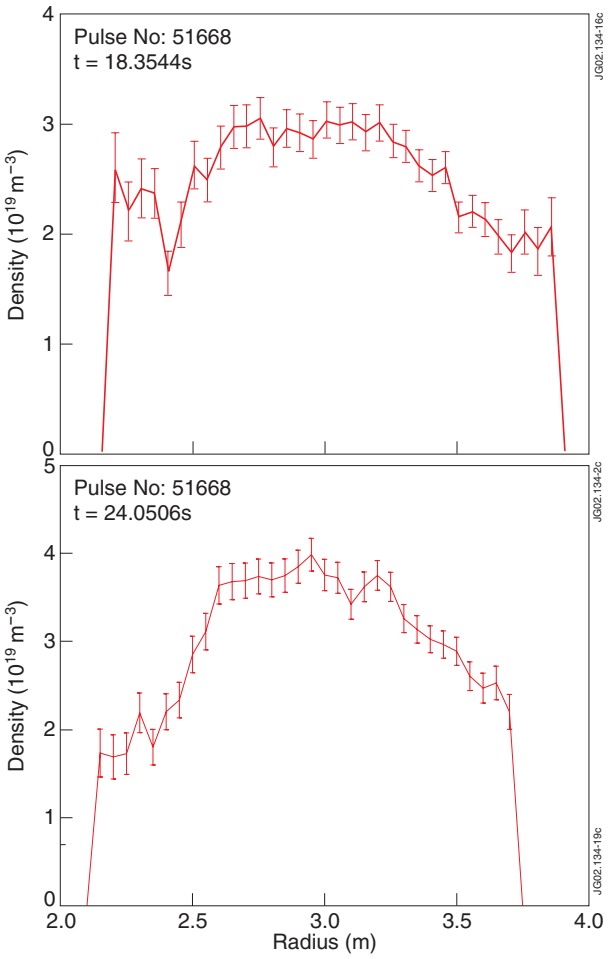

Figure 3a: L-mode Te profile (# 51668 at t=18.35s) Figure 3b: L-mode ne profiles for the same discharge at the same time. Figure 3c: H-mode Te profiles (#51668 at t=24.05s) Figure 3d: H-mode ne profiles for the same discharge at the same time

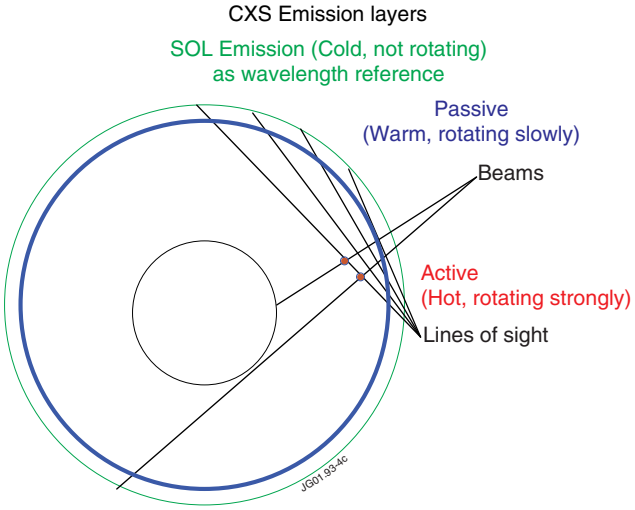

Figure 4: Geometry of the neutral injection beam used for charge exchange and observation view of the CX spectroscopy

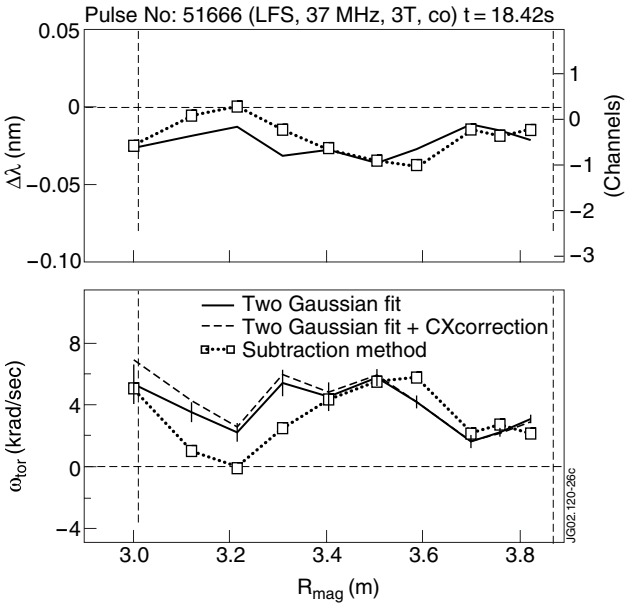

Figure 6: Top: Observed Doppler shift with two analysis methods. Two component fit (solid line) and subtraction method (dotted line). Bottom: Derived frequency of toroidal rotation. The statistical error bar is only shown on the two component fit for clarity, but applies to both methods. In addition we show the effect of correcting the Doppler shift for the CX cross section, again based on the two component fit (dashed line).

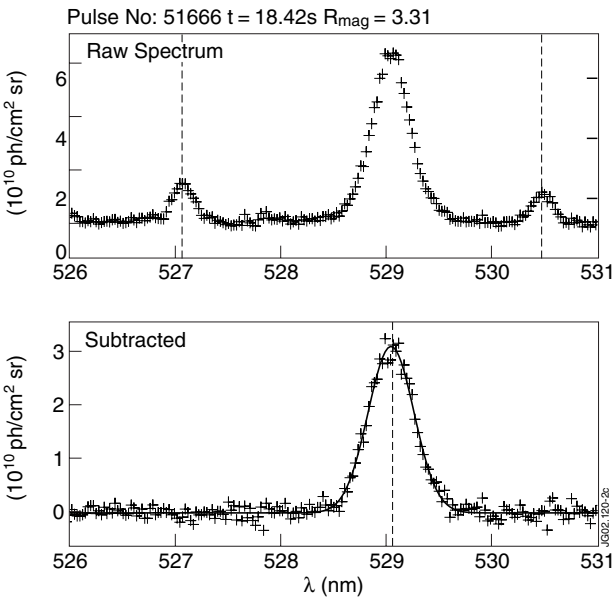

Figure 5: Top: Spectrum of CVI 529.054 nm during NBI, containing cold, warm and hot features. The feature to the left is BeII 527.064 nm (used as a wavelength reference) and the feature to the right is CIII 530.472 nm. Bottom: Difference spectrum due to NBI, generated by subtracting a spectrum prior to the application of NBI. Only the hot component remains.

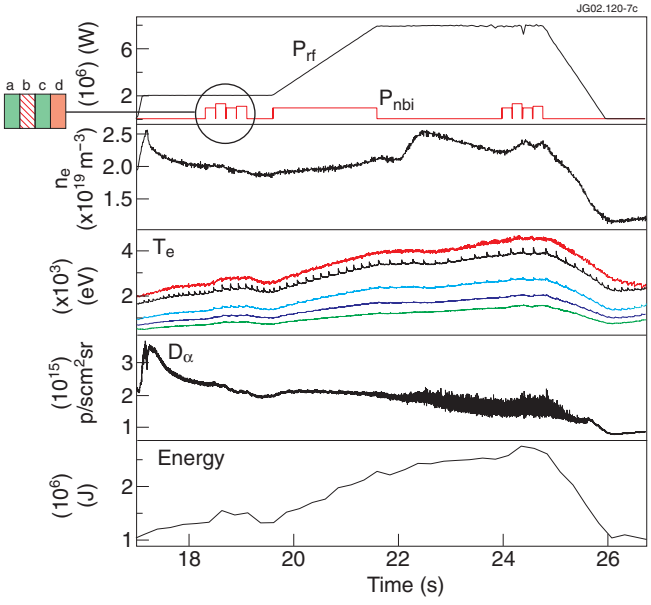

Figure 7: Time traces of (1) the ICRF and NBI power showing the different blips for the measurement, a and c are tangential NBI sources with 140 kV used for the toroidal rotation measurement, b and d are NBI sources with 80 kV (2) line averaged density, (3) electron temperature at several radii, (4) D alpha signal, (5) plasma energy

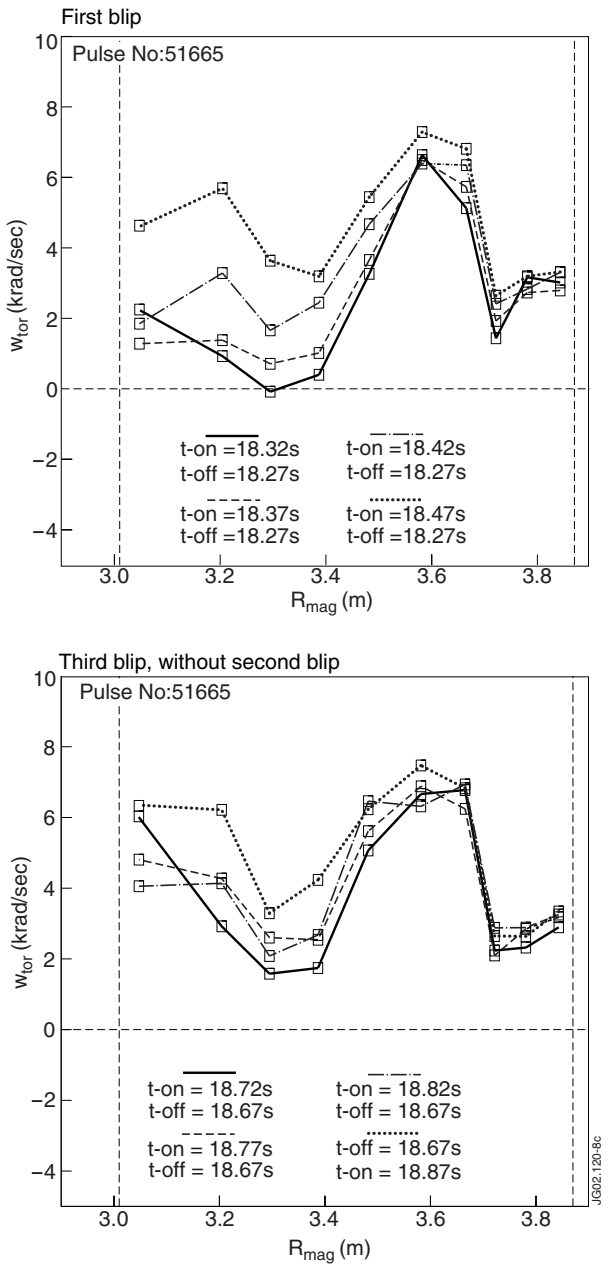

Figure 8: Variation of the rotation profile, (a) during the first beam blip and (b) during the third blip, in the absence of a second blip (#51665, 2.8 T, 51 MHz, counter-spectrum), In both cases the plasma was in the L-mode. Four rotation profiles taken during a time interval of 200 ms are shown. As discussed in the text, the first profile (in bold continuous line) is not markedly influenced by the momentum input of the beam. In this figure, as in all following ones of the rotation profiles, the times (t-on) of the measurement is indicated. The time (t-off) is the time with the beam blip off, that was used in the substraction method for the spectrum which was deducted as explained in section 3.2.

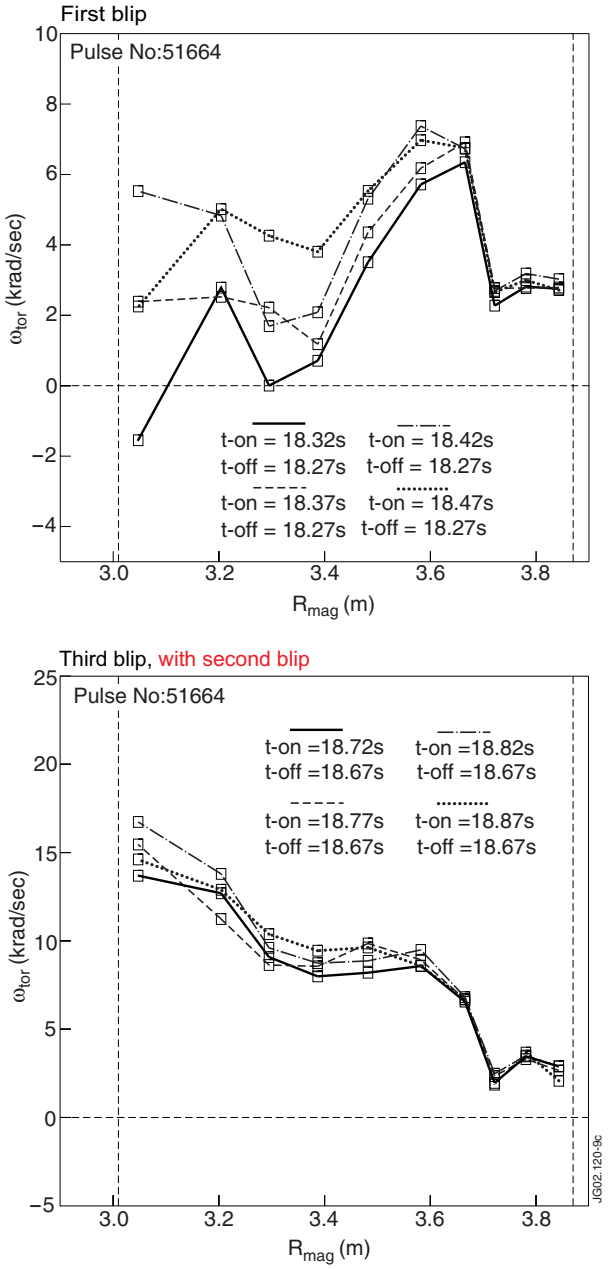

Figure 9: Variation of the rotation profile, (a) during the first beam blip and (b) during third blip, in the presence of a second blip (# 51664, 2.8 T, 51 MHz, co-spectrum)

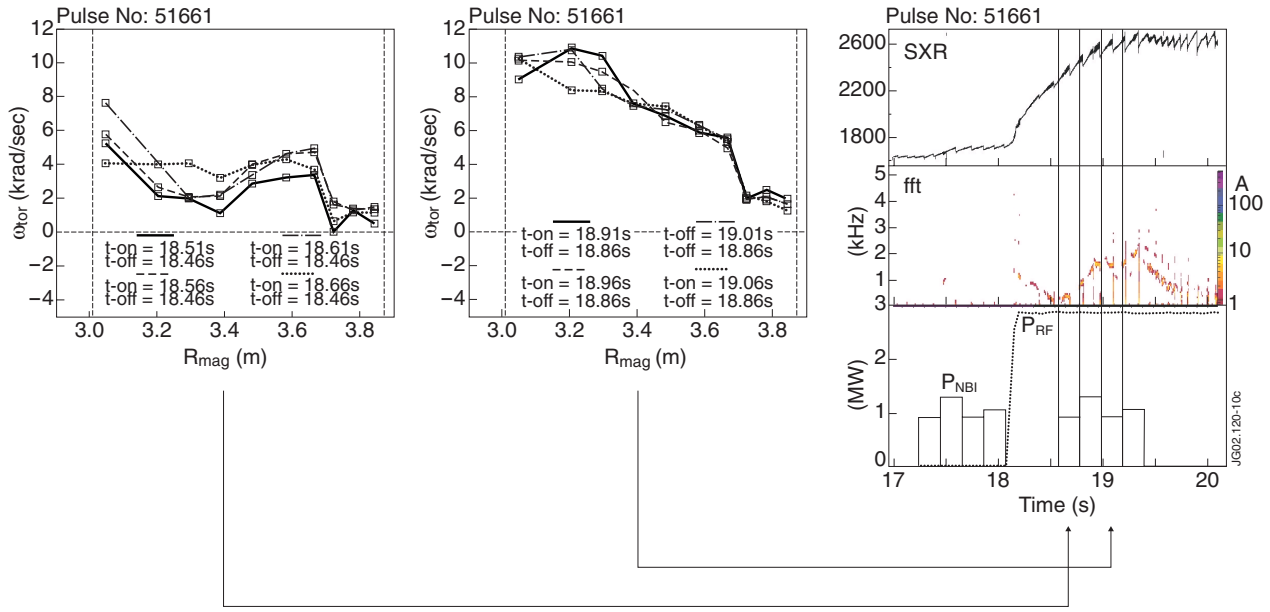

Figure 10: On the right, traces of a central soft X-ray channel (SXR) , its fast fourier spectral analysis (fft) , and the NBI power blips. On the right the measured rotation profiles at the times indicated for pulse #51661. Note the evolution of the central rotation as indicated by the spectral analysis during the NBI blip, and the agreement between the central rotation measured from the soft X-ray and the CX spectroscopy

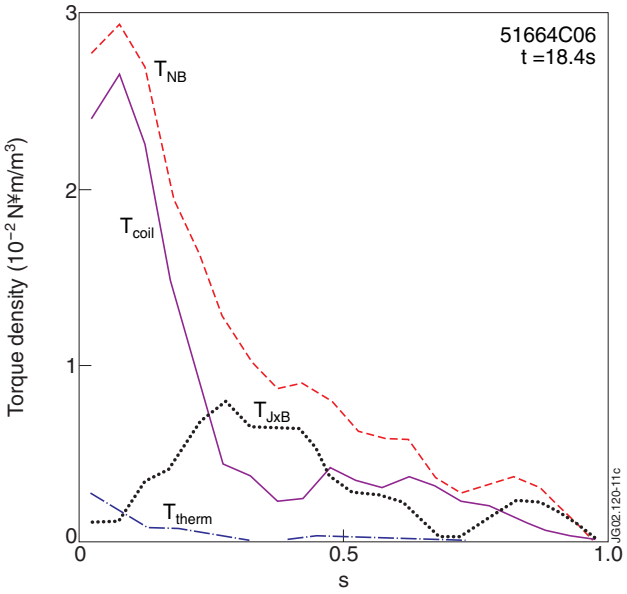

Figure 11: Components of the NBI torque from the NBI blip used for the measurement. The horizontal axis is the square root of the normalized toroidal flux.

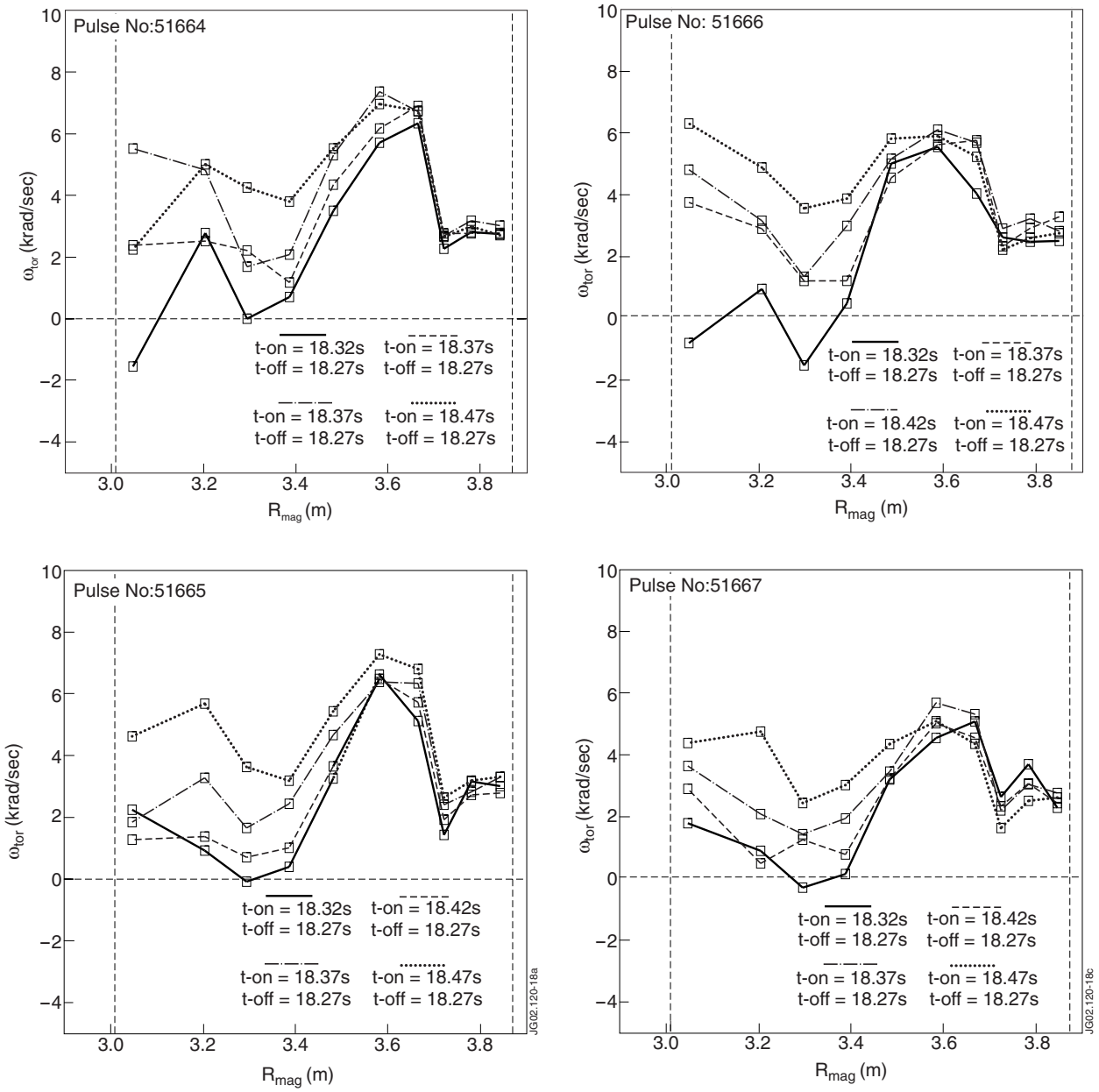

Figure 12a: Rotation profile, for a HFS position of the resonance layer (51 MHz, 2.8T), for a co (top figure, # 51664) and counter directed spectrum (bottom figure, # 51665). Figure 12b:Rotation profile, for a LFS position of the resonance layer (37 MHz, 2.8T), for a co (top figure, # 51666) and counter directed spectrum (bottom figure, # 51667).

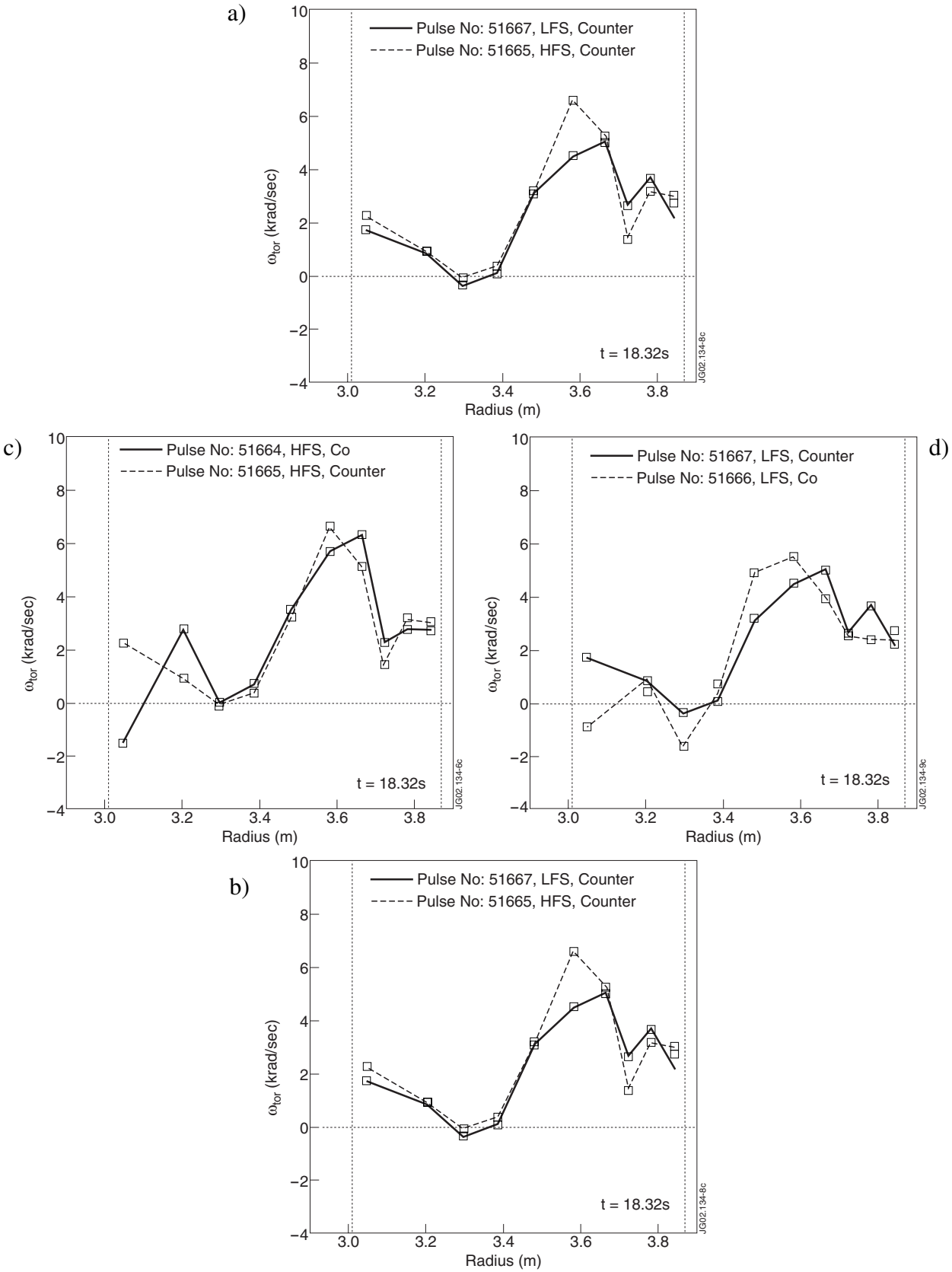

Figure 13a:direct comparison between a HFS and LFS position of the resonance layer for the first profiles for a co-directed spectrum Figure 13b: direct comparison between a co- and counter- directed spectrum for the first profiles for HFS position of the resonance layer Figure 13c Fig. 13 (d) direct comparison between a co- and counter- directed spectrum for the first profiles for LFS position of the resonance layer Figure 13ddirect comparison between a HFS and LFS position of the resonance layer for the first profiles for a counter-directed spectrum

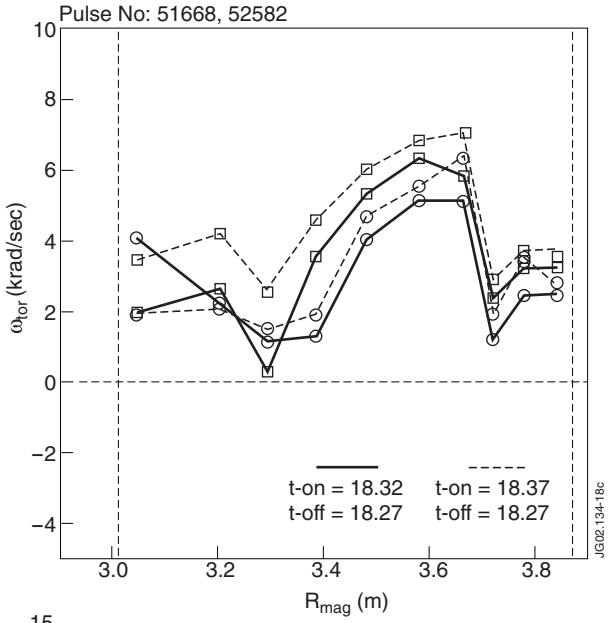

Figure 14:Comparison of the first two profiles of two shots : #51668 (2.8T) with circles, has a co-directed spectrum on the HFS (51 MHZ) and a counter-directed at th LFS (37 MHz ,# 52582 (2.8 T) with squares, has the oppposite, namely a counter-directed spectrum on the HFS and a co-directed on the LFS.

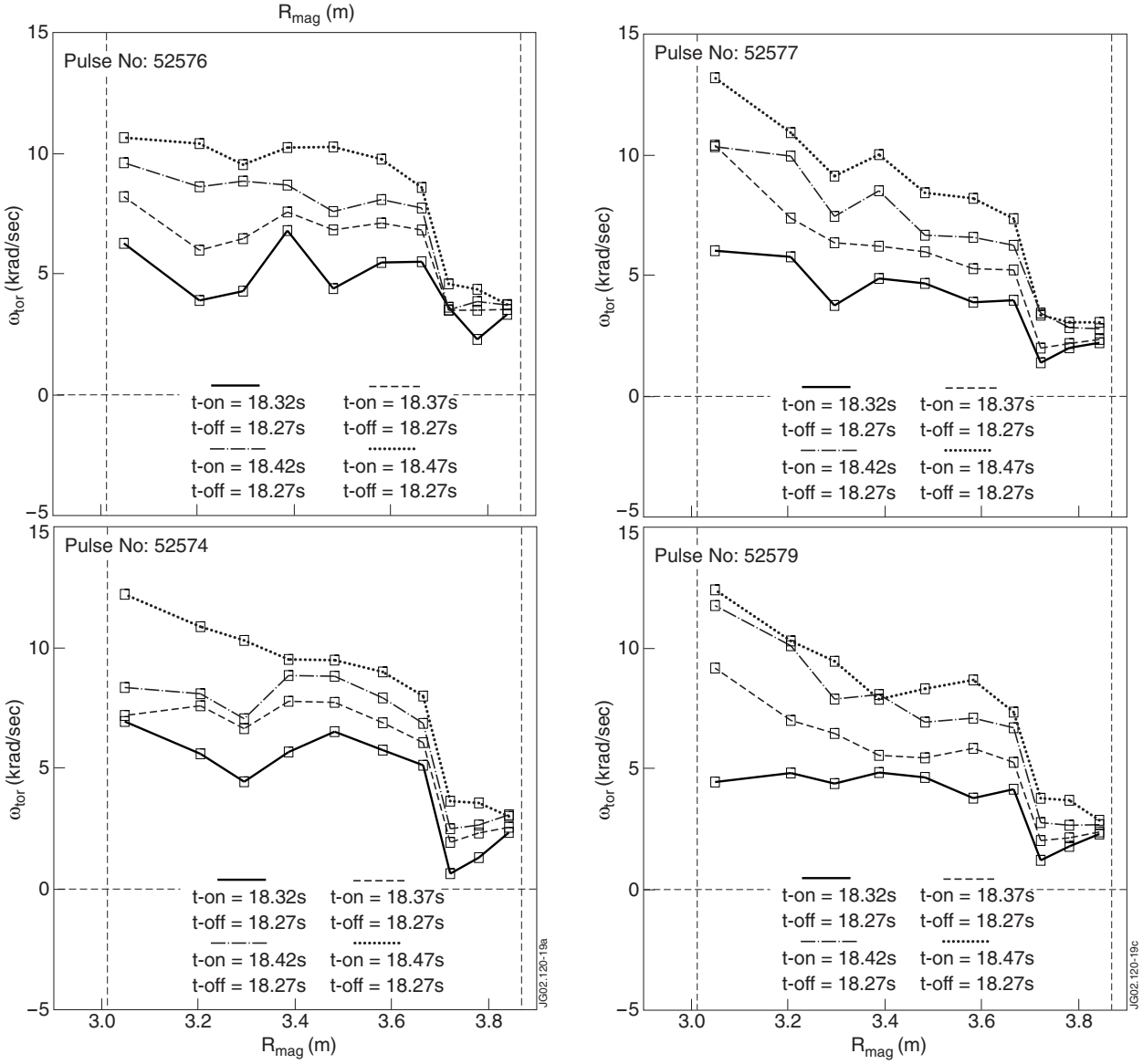

Figure 15a: Comparison of different spectra, all shots with 2.45 T and 42 MHz. (a) # 52576 has a co-directed spectrum Figure 15b: # 52574 has a symmetric spectrum spectrum with 0,π,π,0 Figure 15c: # 52577 has a counter-directed spectrum Figure 15d: # 52579 a symmetric spectrum with 0,π,0,π

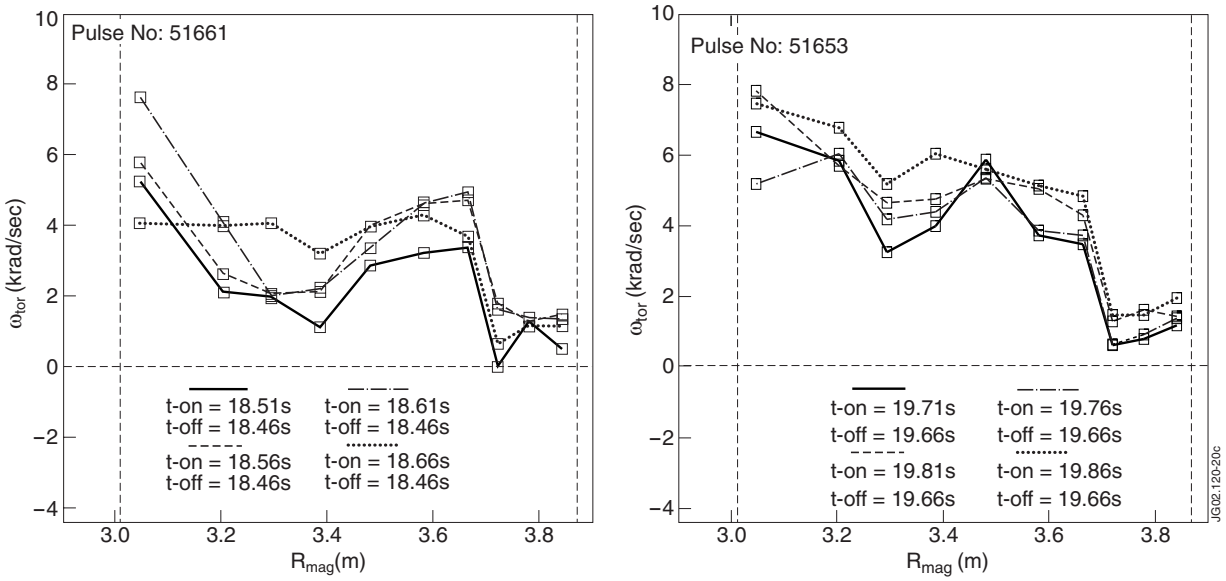

Figure 16: (a) on the left (a) # 516611, rotation profile for a location of the resonance layer at R = 2.59 m, (b) on the right # 51653, for a location of the resonance layer at R= 2.73 m

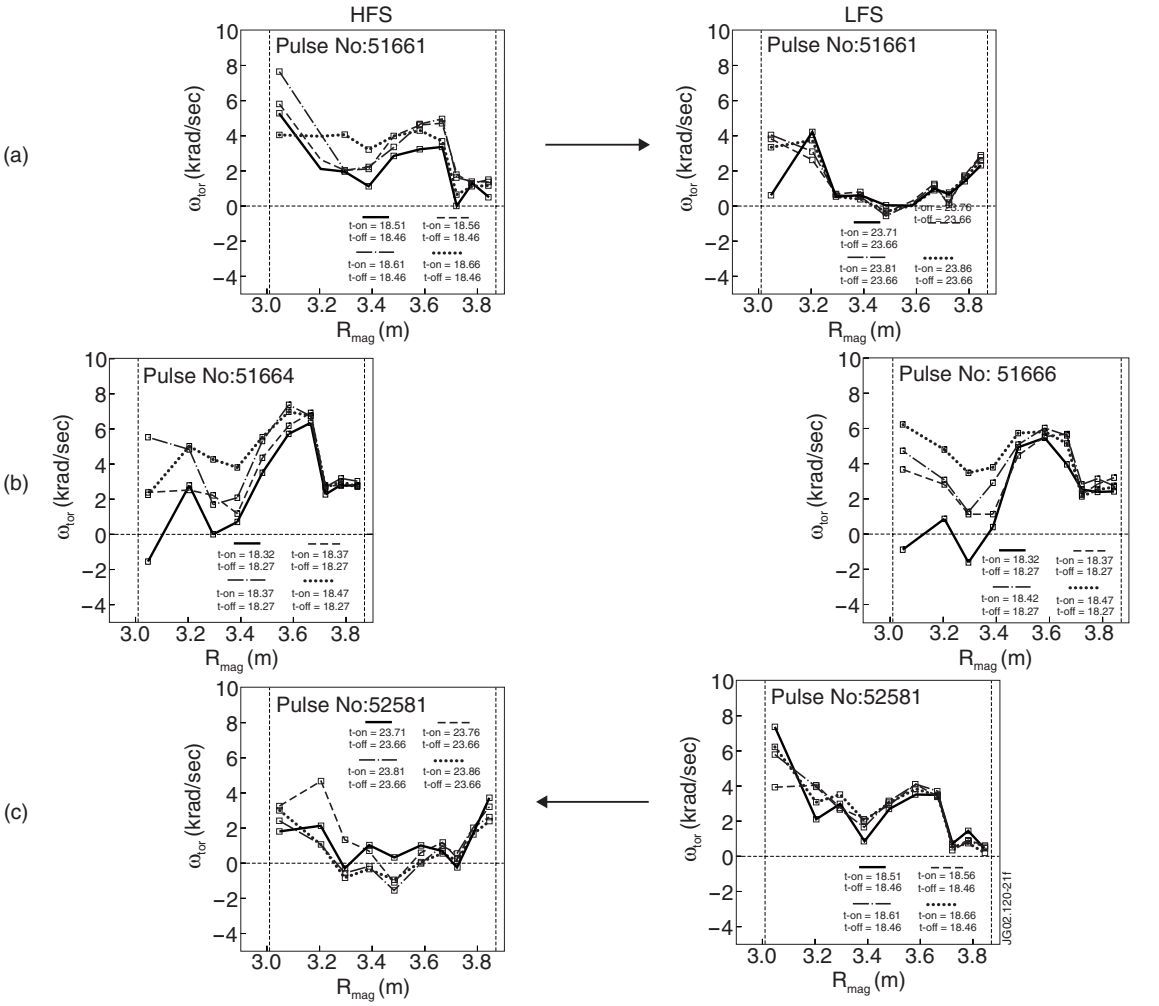

Figure 17: This figure compares the rotation profiles for a HFS and LFS position of the resonance layer obtained by different methods. (b) is obtained by keeping the magnetic field constant, and varying the frequency, in 2 different discharges, (a) by keeping the frequency constant and increasing the magnetic field (in one discharge, thus moving the resonance layer from the HFS to the LFS (c) was obtained in the opposite way : by decreasing the magnetic field during a discharge thus moving the resonance layer from the LFS to the HFS. The location of the different figures in horizontal direction is symbolically a graphic indication of the position of the resonance layer.

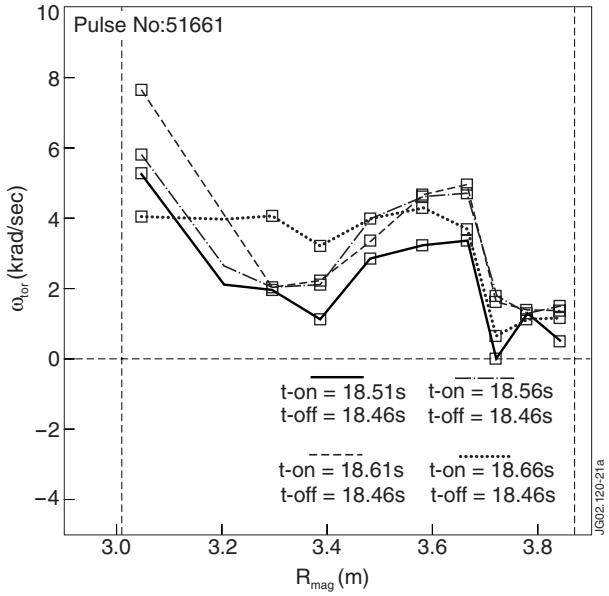

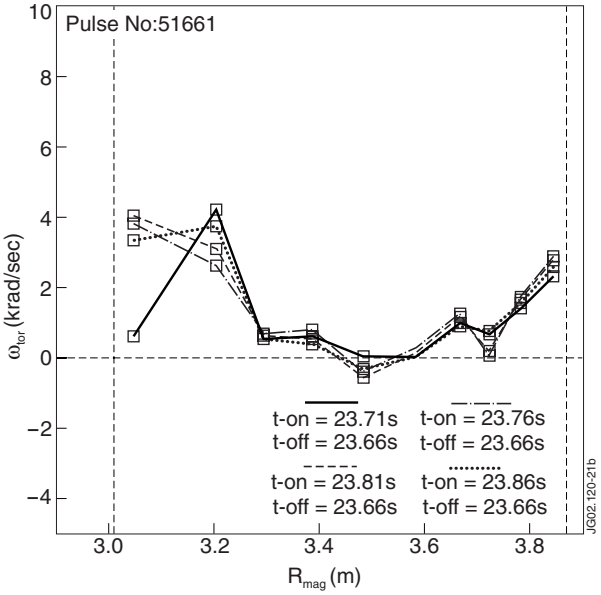

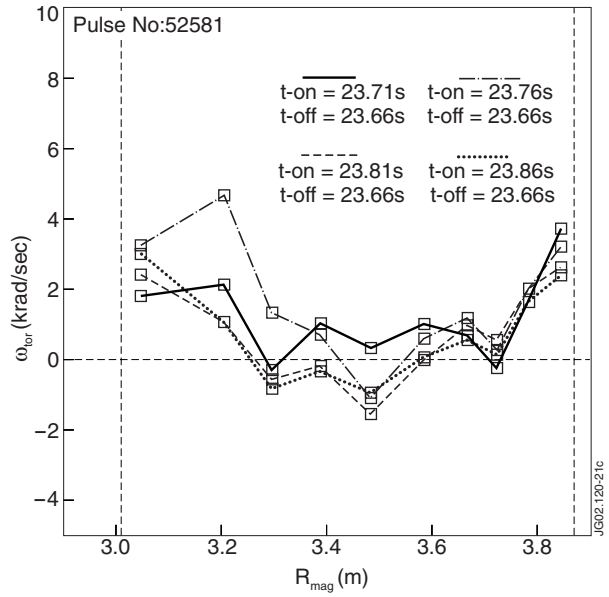

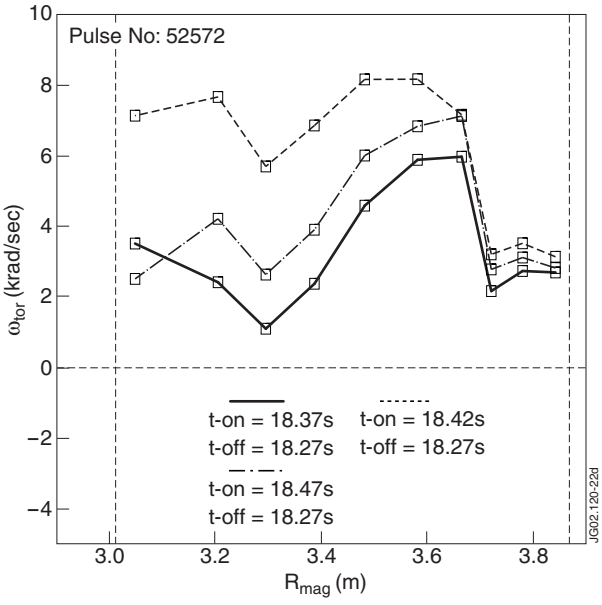

Figure 18: Effect of the concentration, all shots for a HFS position of the resonance layer (2.8 T, 51 MHz) (a) # 51664 for a co-directed spectrum and a low H concentration. Figure 18b: # 51665 for a counter-driected spectrum and a low H concentration. Figure 18c # 52571 for a symmetric spectrum, (0,π,π,0) , and a higher concentration. Figure 18d # 52572 similar to # 52571 , a symmetric spectrum, (0,π,π,0) , and a higher concentration but two beams were used for the measurement, leading to a faster evolution of the profiles.

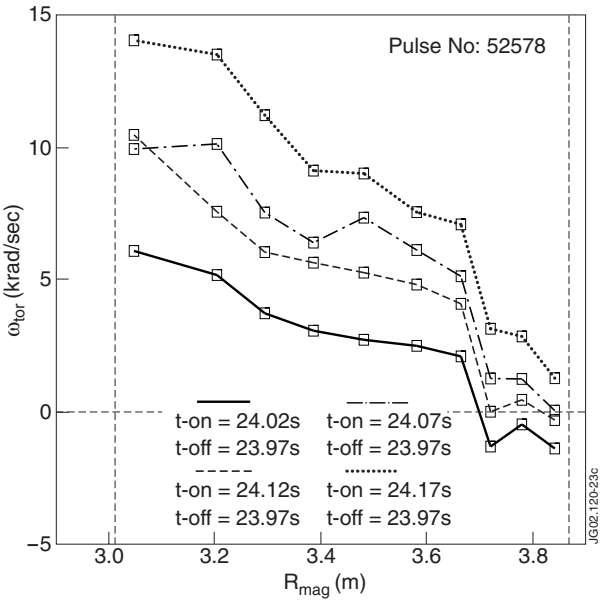

Figure 19: Toroidal rotation profile for # 52578, B= 2.45 T, f= 42 MHz, (R = 2.70 m), P_{IC} = 9 MW, the plasma is in the H-mode.

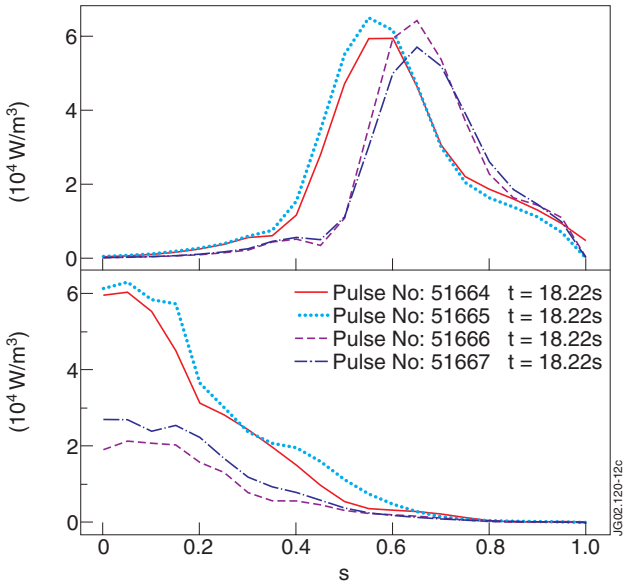

Figure 20: Power density absorbed by (a) hydrogen and (b) direct electron damping as given by PION for discharges 51664-51667 at t = 18.2 s. The horizontal axis is s = sqrt(psi_p/ psi_pa) where is the psi_pa is the poloidal flux at the plasma edge. This is approximately equal to r/a where r/a is the normalised minor radius

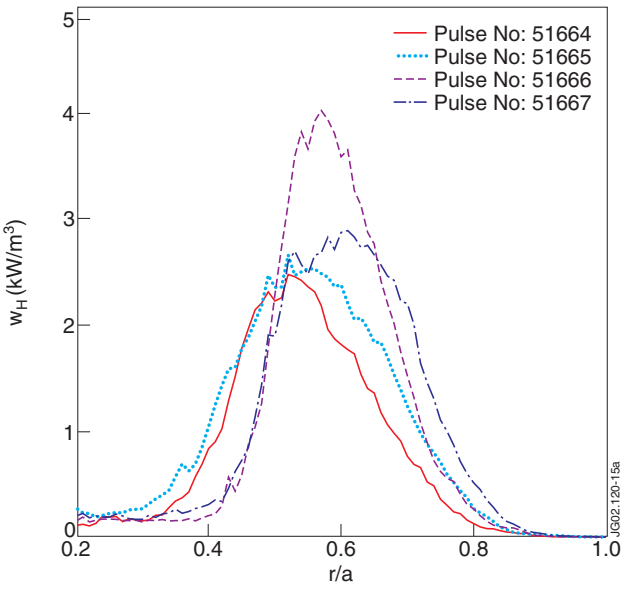

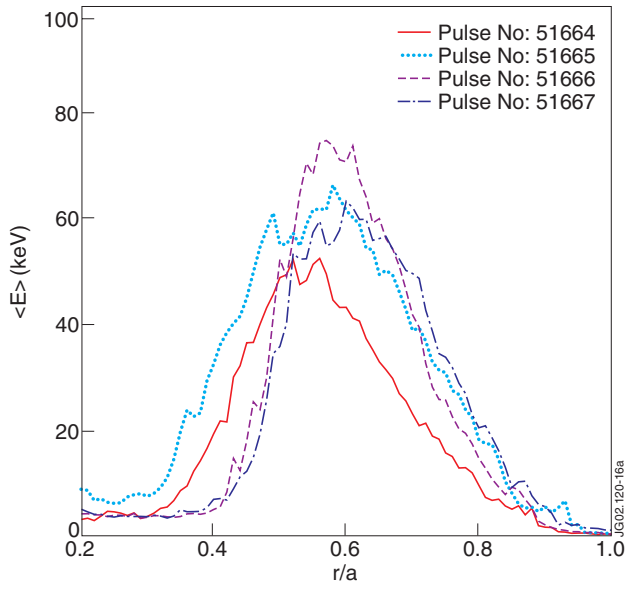

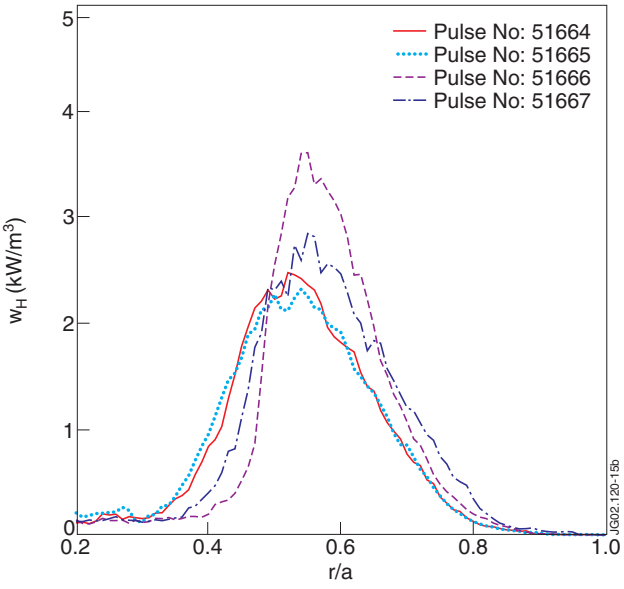

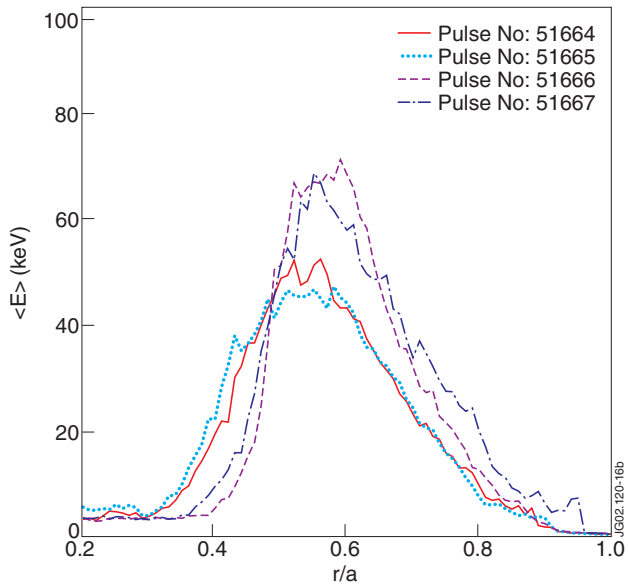

Figure 21: Total energy density in the proton vs normalised minor radius for discharges 51664-51667 as given by the FIDO code at t = 18.3 s. In (a) the measured background plasma parameters of the individual shots have been used. The line styles are as in Figs 20
Figure 21 (b) Total energy density in the proton vs normalised minor radius for discharges 51664-51667 as given by the FIDO code at t = 18.3 s The measured data of discharge 51664 have been used for all discharges.

Figure 22: Mean energy of the protons vs normalised minor radius for discharges 51664-51667 as given by the FIDO code at t = 18.3 s. In (a) the measured background plasma parameters of the individual shots have been used Figure 22 (b) Mean energy of the protons vs normalised minor radius for discharges 51664-51667 as given by the FIDO code at t = 58.3 s. The measured data of discharge 51664 have been used for all discharges.

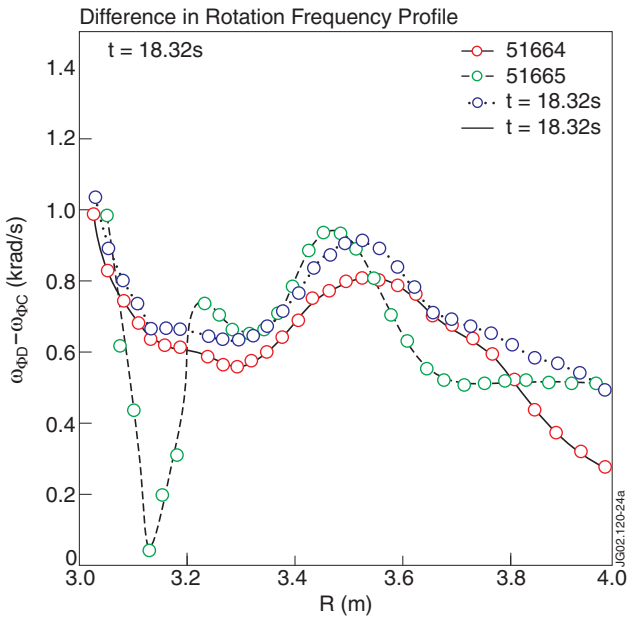

Figure 23: Difference in toroidal rotation frequency calculated using neoclassical theory between C (measured) and D for # 51664 (HFS, co-spectrum)

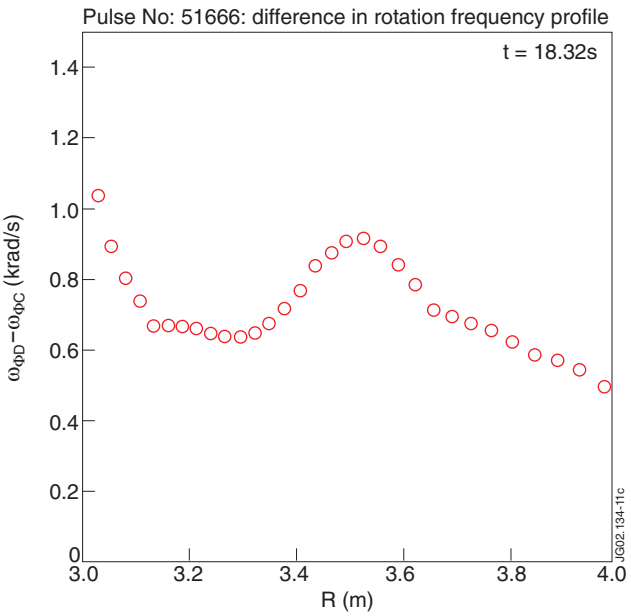

Figure 25: Difference in toroidal rotation frequency calculated using neoclassical theory between C (measured) and D for # 51666 (LFS, co-spectrum)

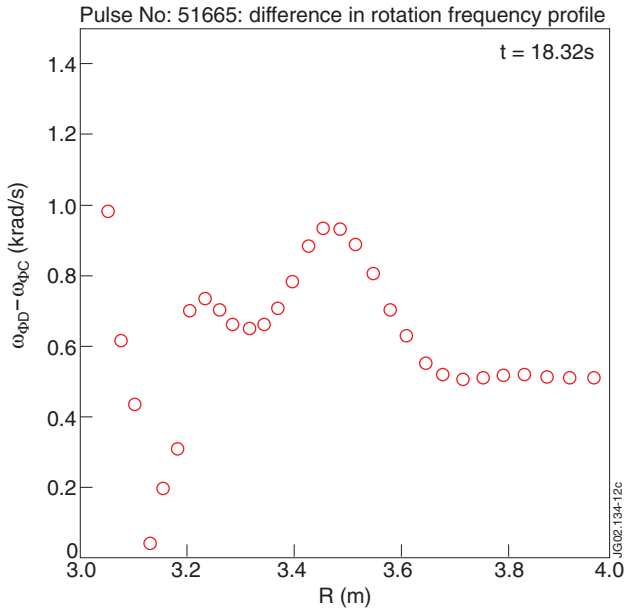

Figure 24: Difference in toroidal rotation frequency calculated using neoclassical theory between C (measured) and D for # 51665 (HFS, counter-spectrum)

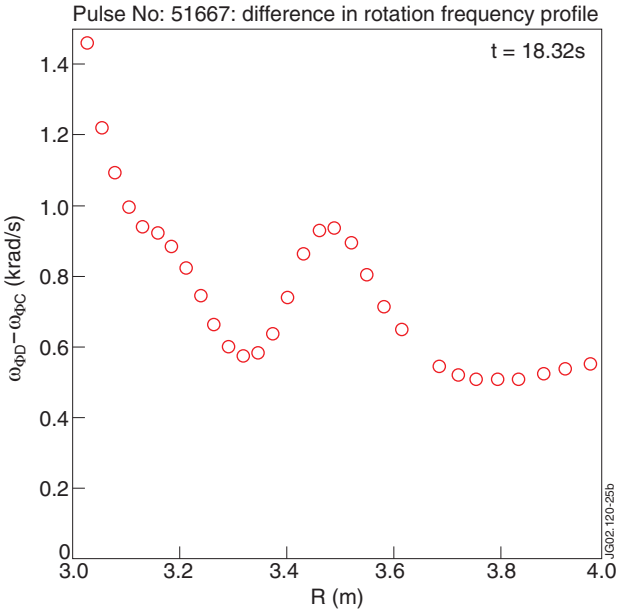

Figure 26: Difference in toroidal rotation frequency calculated using neoclassical theory between C (measured) and D for # 51667 (LFS, counter-spectrum)